PROMISING RESULTS FROM THREE NASA SBIR SOLAR ARRAY TECHNOLOGY DEVELOPMENT PROGRAMS

Mike Eskenazi, Steve White, Brian Spence, Mark Douglas, Mike Glick, Ariel Pavlick, and David Murphy
ABLE Engineering, Goleta, CA 93117

Mark O'Neill and A.J. McDanal
ENTECH Inc., Keller, TX 76248

Michael Piszczor
NASA Glenn Research Center, Cleveland, OH 44135

ABSTRACT

Results from three NASA SBIR solar array technology programs are presented. The programs discussed are the 1) Thin Film Photovoltaic UltraFlex Solar Array; 2) Low Cost/Mass Electrostatically Clean Solar Array (ESCA); and 3) Stretched Lens Array SquareRigger (SLASR). The purpose of the Thin Film UltraFlex (TFUF) Program is to mature and validate the use of advanced flexible thin film photovoltaics blankets as the electrical subsystem element within an UltraFlex solar array structural system. In this program operational prototype flexible array segments, using United Solar amorphous silicon cells, are being manufactured and tested for the flight qualified UltraFlex structure. In addition, large size (e.g. 10 kW GEO) TFUF wing systems are being designed and analyzed. Thermal cycle and electrical test and analysis results from the TFUF program are presented. The purpose of the second program entitled, "Low Cost/Mass Electrostatically Clean Solar Array (ESCA) System," is to develop an Electrostatically Clean Solar Array meeting NASA's design requirements and ready this technology for commercialization and use on the NASA MMS and GED missions. The ESCA designs developed use flight proven materials and processes to create a ESCA system that yields low cost, low mass, high reliability, high power density, and is adaptable to any cell type and coverglass thickness. All program objectives, which included developing specifications, creating ESCA concepts, concept analysis and trade studies, producing detailed designs of the most promising ESCA treatments, manufacturing ESCA demonstration panels, and LEO (2,000 cycles) and GEO (1,350 cycles) thermal cycling testing of the down-selected designs were successfully achieved. The purpose of the third program entitled, "High Power Platform for the Stretched Lens Array," is to develop an extremely lightweight, high efficiency, high power, high voltage, and low stowed volume solar array suitable for very high power (multi-kW to MW) applications. These objectives are achieved by combining two cutting edge technologies, the SquareRigger solar array structure and the Stretched Lens Array (SLA). The SLA SquareRigger solar array is termed SLASR. All program objectives, which included developing specifications, creating preliminary designs for a near-term SLASR, detailed structural, mass, power, and sizing analyses, fabrication and power testing of a functional flight-like SLASR solar blanket, were successfully achieved.

1. NASA SBIR PHASE 2 THIN FILM PV ULTRAFLEX PROGRAM

1.1 INTRODUCTION

As flexible thin film photovoltaic (FTFPV) cell technology is developed for space applications, integration into a viable solar array structure that optimizes the attributes of this cell technology is critical. An advanced version of the ABLE Engineering, Inc. (ABLE) UltraFlex solar array platform represents a near-term, low-risk approach to demonstrating outstanding array performance with the implementation of FTFPV technology. Recent studies indicate that an advanced UltraFlex solar array populated with 15% efficient thin film cells can achieve over 250 W/kg BOL.

ABLE, in collaboration with the NASA Glenn Research Center (GRC), is currently executing a NASA Phase 2 Small Business Innovation Research (SBIR) program to implement and validate the integration of FTFPV technology within an advanced UltraFlex solar array [1]. The primary objectives of the Phase 2 SBIR program are to mature and validate the use of advanced FTFPV blankets as the electrical subsystem element within an advanced UltraFlex solar array structural system. Program objectives to mature and validate the use of FTFPV blankets in the UltraFlex solar array platform are being met though the implementation of a hardware oriented development and test approach (at the coupon and engineering model level).

As has been recognized in recent array system level studies [2], integration of a FTFPV electrical subsystem into an advanced UltraFlex solar array structural system allows realization of the full potential of FTFPV technologies to increase solar array specific power and significantly reduce cost. While the prior research focus has been aimed at the FTFPV device level in an effort to improve BOL/EOL efficiencies, reduce weight, and enhance space environmental survivability [2, 3], the development, implementation and validation of these technologies within a viable lightweight array system (including the "real world" effects on specific power performance from array wiring, structures and deployment mechanisms) has been only superficially addressed prior to this Thin-Film UltraFlex SBIR study. Validating the successful combination of a structurally/mechanically efficient advanced UltraFlex solar array platform with the unique properties of FTFPV technology is a key step in maturing these technologies and readying their space commercialization.

During this NASA Phase 2 SBIR program preliminary design/analysis activities have been performed for a high performance thin film PV UltraFlex solar array system configured for a 10kW EOL GEO application. Feasible design solutions for high voltage operability, scalability, optical characteristics, high thermal performance, and radiation survivability have been identified. Coupon development and hardware tests have been performed on flight-like FTFPV gore/blanket assemblies to validate concept/design feasibly. Larger scale flight-like engineering model hardware has been built to further validate design manufacturing, packaging and deployment feasibility at the wing system level.

1.2 TECHNOLOGY OVERVIEW

The UltraFlex solar array, shown in Figure 1, combines structural performance and the highest available specific power with a very low stowed volume and footprint [3]. The UltraFlex achieves its deployed strength and stiffness from lightweight composite radial spar members that allow tensioning of a flexible blanket populated with photovoltaic. This unique structural system allows the use of a flexible blanket without requiring massive secondary structure to deploy and tension the wing as is common in other flexible substrate solar array systems. UltraFlex is an excellent platform to demonstrate maximum specific power performance gains from high areal mass-efficient thin-film photovoltaics because of its superior areal structural mass efficiency that is up to 3.5X better than a conventional rigid planar array.

Figure 1. UltraFlex Solar Array for the Mars 01-Lander Program

The UltraFlex is an accordion-fan-fold flexible solar array composed of ten interconnected isosceles triangular shaped lightweight substrates (gores). The fan-fold geometry sequences the gore blanket assemblies during deployment. Each interconnected triangular shaped substrate/gore unfolds to form a tensioned ten-sided polygon structure when fully deployed. Radial spar elements attached to each substrate are elastically deflected to form a tension-preloaded concave paraboloid, providing high-deployed strength and stiffness. A layout of the deployed UltraFlex depicting its major components is shown in Figure 2.

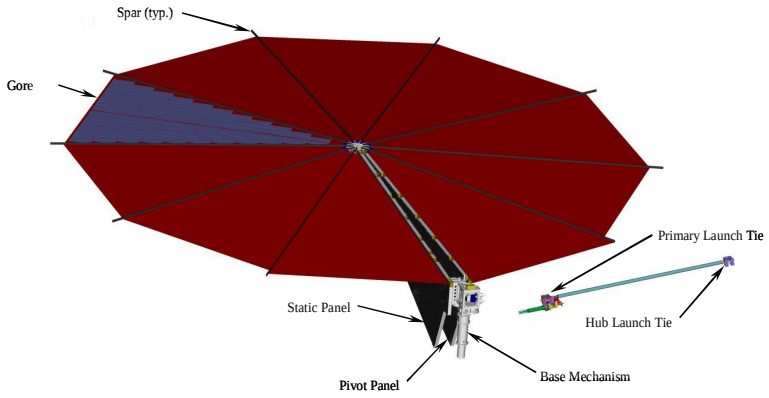

Figure 2. UltraFlex Wing Components

When stowed, the UltraFlex occupies a triangular space that is approximately 20% the stowed volume of conventional planar arrays, which enables spacecraft to maximize launch volume for critical payloads. The honeycomb-composite static and pivot panels sandwich and preload the folded solar array blanket under pressure in the stowed configuration. In a standard crystalline photovoltaic-based design, the UltraFlex wing's solar cells are protected from damage in the launch environment by foam interleaved in the folded blanket assembly. The stowed and compressed wing assembly is held to the space vehicle at three releasable launch tie points. Figure 3 shows the stowed UltraFlex configuration.

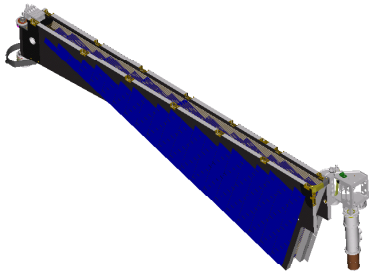

Figure 3. UltraFlex Stowed Configuration

1.3 FLEXIBLE THIN FILM PV (FTFPV)

The primary suppliers and technologies under consideration during this program included United Solar Systems' (USS) amorphous silicon (α-Si) FTFPV, and ITN Energy Systems' CIGS FTFPV technology. At program commencement, due to limited funding, only the USS α-Si technology was selected for implementation and test. Additional funding was obtained later in the program, and ITN Energy Systems CIGS will be included in similar coupon-level and engineering model level development tests to be performed in early 2004.

The baseline α-Si FTFPV technology utilized for this program was USS "Q" solar cell. The "Q" cells are produced on a 25 micron (0.001-inch) thick stainless steel substrate, have a Ag/ZnO back reflector, a top side Indium-Tin-Oxide (ITO) coating, and are tuned to the 1AM0 solar spectrum. The top surface conductive grid consists of a series of longitudinally oriented small diameter compression-bonded copper wires. The wires are terminated/connected to a silver coated copper bus that is used for cell-to-cell series interconnection. The cells measure approximately 4-cm X 17.8-cm and have an active area of 64.30 cm^2. The measured mass of each solar cell assembly is approximately 2.37 g (areal density of 0.37 kg/m2). A picture of the a-Si USS solar cell assembly is shown in Figure 4.

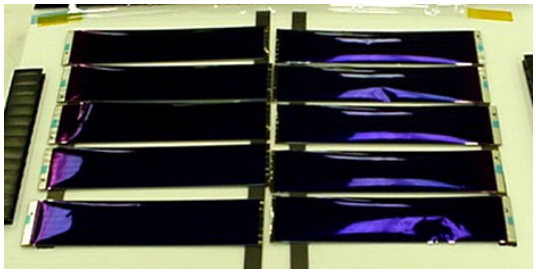

Figure 4. USS a-Si FTFPV ("Q"-cell)

The baseline copper indium gallium diselenide (CIGS) FTFPV technology to be investigated during this program is the ITN Energy Systems Inc. (ITN) space-application solar cell mounted on 1 mil. stainless-steel substrates. ITN Energy Systems has developed a technology that adapts the cell material obtained from Global Solar Energy Inc. (GSE) into a product capable of surviving in a space environment. This is accomplished by adding AM0 optimized space grids, thermal coatings to reduce on-orbit operating temperature and electrostatic discharge layers (ESD) for operation in a plasma environment to the basic cell material obtained from GSE. Additionally, the cells provided by ITN for this program will include ITN's bonded interconnect technology that will allow integrated solar arrays for space applications to be implemented. As previously mentioned, validation of the ITN CIGS technology is currently underway with results anticipated for early 2004.

1.4 THIN FILM ULTRAFLEX HARDWARE DEVELOPMENT & TESTING

1.4.1 Structural Optimization

During this program many of the standard UltraFlex array's structural design features were weight-optimized to take advantage of the FTFPV's significantly lighter weight and robustness versus classical crystalline PV technologies. Because FTFPV technologies are projected to be almost four times lighter than the state-of-the art crystalline multi-junction cells on a weight per unit area basis, and are not subject to cracking or damage from vibratory motion, the method of tightly preloading the folded gore stack between layers of foam does not appear to be necessary with this technology. This allows the UltraFlex static and pivot panels (nominally of honeycomb-composite construction) to be further weight-optimized for use as stowed protective covers and deployed structural members, without the considerable stiffness and strength required to apply a uniformly-distributed preload over the stowed stack area, which is necessary for crystalline PV applications. ABLE has developed a concept for a lightweight iso-grid static and pivot panel construction that allows the panel stiffness to be tailored specifically for a low mass stowed FTFPV blanket stack. This panel construction saves significant weight (20-40%), especially when scaling UltraFlex to the larger sizes (>4m diameter) required when implementing lower efficiency FTFPV.

An alternate approach to reduce the weight of the static and pivot panel structure on large FTFPV UltraFlex wing configurations is to increase the number of launch tie locations so that the panels do not have to be as stiff and strong to apply preload to the stowed blanket stack. This concept requires the implementation of a weight-optimized launch tie assembly. The baseline UltraFlex launch tie is based on the heritage ABLE launch release that uses high-output paraffin actuators to release a tensioned cable. This design has extensive flight heritage and works well for applications requiring three or less tie-down release points, but would add unnecessary weight if applied at multiple (>4) launch tie points. For a larger-diameter FTFPV UltraFlex application requiring more launch tie locations, ABLE has initiated development of a next-generation launch tie release that utilizes small lightweight discrete bolt-separation actuators at each tiedown location. During this Phase 2 SBIR program, such a weight optimized launch tie release was considered in the FTFPV UltraFlex array sizing trades, with results indicating they have the potential to significantly reduce mass versus the existing launch tie technology, as well as reducing the necessity for ultra-stiff (and massive) structural panels.

Additionally, the radial spar elements can be structurally optimized for FTFPV applications. With lightweight FTFPV technology the spar structures do not need to support as much weight when deploying or in the fully deployed configuration (under 1-G ground-test conditions). The standard UltraFlex design utilizes a flat rectangular composite spar construction with the lay-up optimized to support deployment loads under 1-G with minimal external support. A FTFPV array, with significantly larger wing area required for the same power output,

will require an external ground support structure to allow deployment under earth gravity. A rectangular spar applied to such a large wing could be susceptible to torsional instability and could buckle even when supported under 1-G unless it becomes very large and heavy. The design of a large TFTPV wing required re-assessment of the spar's design to provide the most weight-optimal cross section that can still be packaged in the stowed configuration. ABLE has investigated concepts for deployable "lenticular" spar sections that stow in a flat package but expand out when deployed to form a very lightweight, torsionally stiff beam section that is less susceptible to lateral/torsional instability.

1.4.2 Interconnect Development and Testing

Previous solar array system studies suggest that a monolithically interconnected FTFPV blanket assembly is needed to truly realize the cost and mass benefits potential of this technology [1]. Because monolithic interconnection of FTFPV is still in development this technology was not available to implement on this program. Instead, the FTFPV interconnection technologies developed during this program focused on classical welding and soldering approaches.

Because the UltraFlex blanket/gore assemblies are stowed face-to-face it is desirable to employ an interconnect that exhibits very low profile. To satisfy this need two interconnect approaches were ultimately pursued, a folded-flexible type that provided large stress relief and an in-plane type. A representative folded flexible interconnect prototype mock-up was made and tested for flexibility in two directions. The interconnect consisted of a folded copper strip that was welded to the top and bottom of adjacent cells. The fold in the copper strip allows the interconnect to flex during expansion and contraction of the circuit during thermal cycling. The folded interconnect testing successfully demonstrated the durability and flexibility of the design concept. A picture of the mechanical fold interconnect mock-up is shown in Figure 5. A prototype in-plane interconnect was also made and evaluated by ABLE and USS. The in-plane interconnect consisted of a straight copper strip that was welded to the top and bottom of adjacent cells using multiple welds. The in-plane interconnect testing successfully demonstrated the durability of this design. The results of this interconnect development effort indicated that either in-plane or stress-relief interconnects were suitable for UltraFlex and should be evaluated at the flight-like coupon level using the α-Si FTFPV.

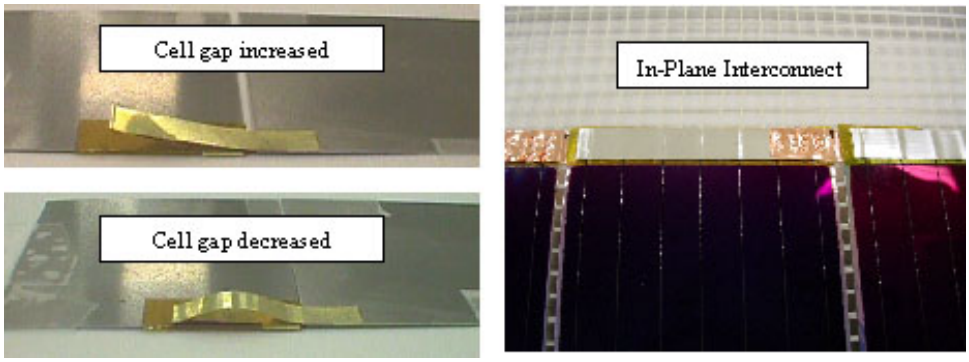

Figure 5. Folded-Flexible Interconnect Detail (Left) and In-Plane Interconnect Detail (Right)

The ITN CIGS cells will be interconnected using an adhesive bonding interconnect technology that combines the strength of a mechanical bond (to carry the CTE mismatch induced stress) with the electrical conductivity of a conductive bond. This interconnect design will be tested by ITN and ABLE to demonstrate the thermal-cycle durability of the design.

1.4.3 Circuit/Laydown Development & Test

To maintain blanket design commonality with previously qualified crystalline PV UltraFlex systems the FTFPV blanket/gore approach is comprised of a mesh substrate to which the interconnected cells are bonded. The amount of cell-to-gore mesh bond area can be significantly reduced, because the lightweight FTFPV will have less of a propensity to de-bond under its own accelerated mass.

An ultra-lightweight method for cell-to-gore mesh attachment was developed that utilized Kapton “dots” bonded directly to the cell backside and the UltraFlex gore/substrate, as shown in Figure 6. This feature resulted in an 80% savings in cell-to-gore adhesive mass over the crystalline UltraFlex design. This low-cost method also provides a significant reduction in laydown assembly time compared to the standard UltraFlex cell attachment method. Engineering development tests were performed on a prototype incorporating this laydown approach to demonstrate concept feasibility. A localized proof load using a small vacuum suction cup was applied to each bonded cell to determine acceptable bond strength. Test results indicate that no bond degradation occurred under the normal load application.

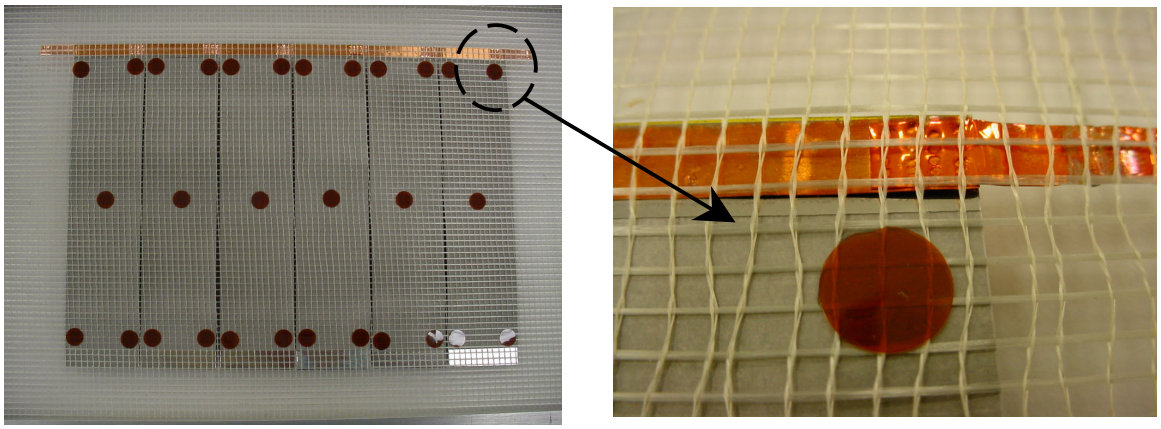

Figure 6. Lightweight Cell-to-Gore Attachment Using Kapton Dots

To further validate the cell/circuit interconnect approach, and circuit laydown, a flight-like engineering mock-up was fabricated. The engineering circuits incorporated the folded flexible interconnect design as well as the baseline in-plane welded interconnect and were mounted to a tensioned UltraFlex blanket/gore segment. The hardware employed the following three circuits: Circuit-1 consisted of three 25-micron-thick dummy cells with straight 100-micron-thick copper strip soldered interconnects, Circuit-2 consisted of two 125-micron-thick cells with a soldered flexure interconnect and improved grid wire terminations, and Circuit-3 consisted of two 125 micron-thick cells with a soldered flexure interconnect and improved (segmented) grid wire termination. The original design for the grid wire terminations consisted of a layer of Kapton tape above and below the grid wires, and this double-layer termination method exhibited significant peeling following limited thermal cycles. An improved approach was developed that utilized a single layer of Kapton tape compression-bonded over the grid wires and to the cell edge surface. Additionally, this grid wire termination tape was segmented into three shorter sections on one of the samples in an effort to reduce thermal stresses and distortion. A photograph of the development circuit hardware is shown in Figure 7. Thermal cycle testing of the engineering gore segment was performed to determine any degradation and validate grid wire termination, cell/substrate attachment, and interconnect integrity/performance. The hardware was thermal cycled for a total of 266 cycles between –175C to +100 C at a rate of 2.5 cycles/hr. Visual inspections and interconnect resistance measurements were made at 55, 104, and 266 cycles. Test results indicated no visible degradation of the straight and flexible interconnect configurations, no change in interconnect resistance, and the cell/substrate attachment was unaffected based on pull test measurements. The improved single layer grid wire termination (segmented and un-segmented) had no visible degradation following 266 thermal cycles. As a result of this testing the improved, segmented approach has been baselined.

`

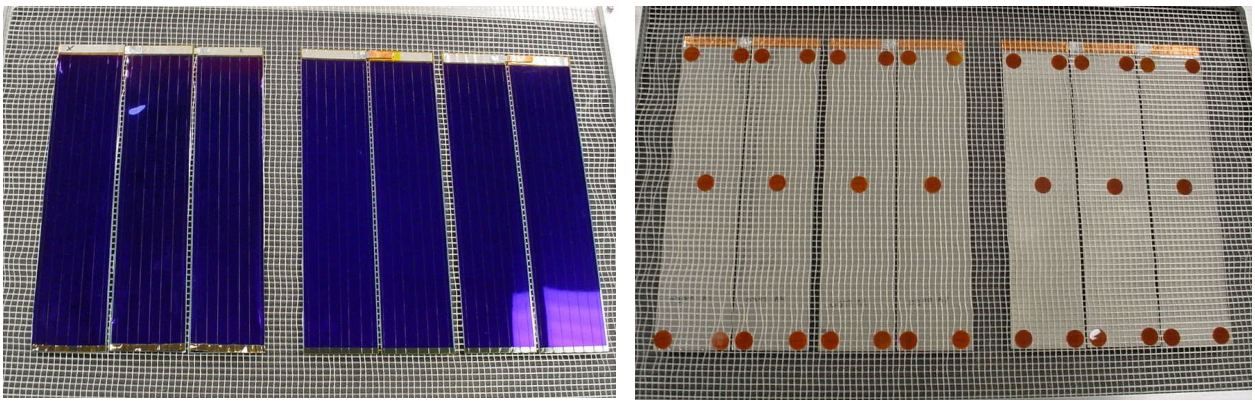

Figure 7. Development Circuits (Front and Back Views)

1.4.4 Thin-Film UltraFlex Engineering Circuit (E-Board) Testing

To further validate FTFPV interconnection and laydown onto UltraFlex, two flight-like engineering circuits (E-Boards) were fabricated. Each circuit consisted of a 6-cell series interconnected a-Si FTFPV assembly bonded to the UltraFlex gore/substrate. Cell thickness was 25 microns (0.001 inch). Each circuit utilized a different interconnect method; the baseline in-plane welded tab design and the folded flexure design. The engineering circuits were inspected and tested with ABLE's Large Area Pulsed Solar Simulator (LAPSS), and then mounted on two separate sections of tensioned UltraFlex gore/blanket using the previously verified Kapton "dot" attachment method. A pre-test electrical LAPSS performance evaluation was performed for the completed assembly. Pictures of the small flight-like E-Boards are shown in Figure 8.

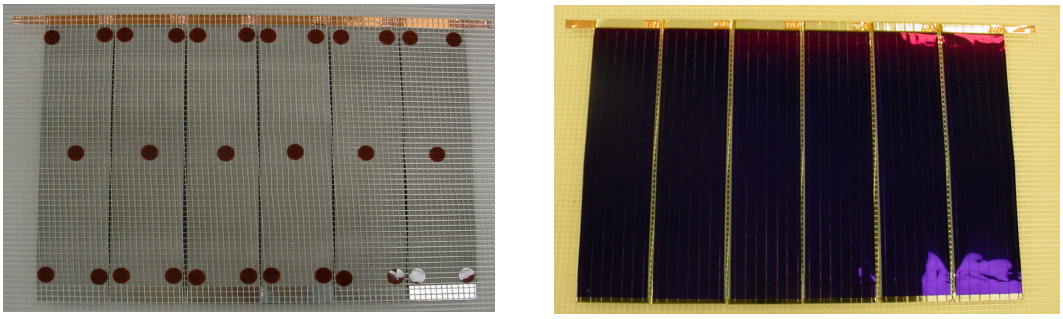

Figure 8. E-Board Circuit on UltraFlex Gore/Substrate

The completed E-boards were then mounted within a thermal chamber and were subjected to 500 thermal cycles at temperatures from -175°C to +100°C. Periodic inspections and continuity monitoring during the thermal cycle tests indicated no apparent degradation/failures of either circuit. Final post-test inspection and LAPSS verification of the circuits were performed, showing both circuits in good condition with only minimal localized physical degradation.

Post-thermal LAPSS testing of the two circuits demonstrated no measurable degradation in cell performance when compared to the pre-thermal LAPSS data. The observed local separation of the Kapton tape and the rear contact on the flexible copper interconnect circuits did not affect the circuit performance. Pull tests on the cell-to-gore/substrate bonds demonstrated that the cell attachment was unaffected by thermal cycling.

The following conclusions were made from the fabrication and testing of the two E-Board circuits:

1) The circuit electrical performance was unchanged by the thermal cycle testing.
2) The straight welded interconnect is generally a good match with the UltraFlex gore/substrate and local attachment of the cell. No interconnect failure resulted from the thermal expansion and contraction of the cells relative to the UltraFlex gore/substrate. The flexible interconnect is probably not required when the cells are attached to the UltraFlex gore/substrate.
3) The number of welds used to attach the rear copper contact to the stainless substrate may need to be increased to prevent the observed separation of the contact from the stainless substrate.
4) The separation of the Kapton tape from the top ohmic points to a required change in surface preparation, tape adhesive, tape type, or material configuration when the cell is required to operate at the tested thermal environment.
5) The cell attachment was generally unaffected by the thermal environment.

1.4.5 Face-to-Face Survivability

An investigation into the surface durability of the α-Si FTFPV modules was performed. This is an area of particular concern for the UltraFlex application because in the nominal stowed configuration, FTFPV cells are in direct face-to-face contact. A number of tests were performed initially to assess the relative durability of the (unprotected) α-Si FTFPV surface, as shown in Table 1. The tested FTFPV cells did not have any anti-reflective or oxide coatings on their front surface. Initial test results indicate that an unprotected front surface of the α-Si FTFPV is highly susceptible to damage from cell-to-cell contact and handling.

Table 1. Surface Durability Test Results of Un-coated FTFPV

Test Description	Test Result
Two cells were placed face-to-face under 0.1 psi pressure	No cell damage
Rounded edge of paperclip placed in contact with cell surface and lightly translated across cell	Cell completely shunted
Two cells were placed face-to-face. Light pressure was applied to top cell and top cell moved relative to bottom cell (displacement ~ .05 in., duration ~ 3 sec).	Cell completely shunted
Two cells were placed face-to-face. Foam was placed over top cell and weights applied to exert 0.1 psi pressure. The assembly was repeatedly moved on granite table (displacement ~ .05 in., duration ~ 3 sec.)	Cell completely shunted

The effectiveness in improving FTFPV durability by employing various thickness SiO_2 coatings applied to the PV front surface was investigated. A number of 4.7" x 14" terrestrial α-Si cells were obtained from USS for use in determining optimal coatings to enhance cell front surface durability. The cells were coated with SiO_2 of thickness varying from 0.1 μm to 3 μm, as shown in Table 2. Additionally, a 0.06 thick ITO layer was applied to the front surface of the cells. The reason for the ITO layer was to eliminate the potential for charge buildup on the SiO_2 surface on orbit. Subsequent discharge from the cell surface may damage the circuit.

Table 2. Matrix of ITO Coating Thickness Applied to Durability Test Cells

Designation	SiO_2 Thickness (μm)	ITO Thickness (μm)
A	0.1	0.06
B	1.0	0.06
C	3.0	0.06

After coating, the electrical performance of the test cells was measured and the durability of the cells was evaluated. One cell was placed on a smooth granite surface with the PV side facing upward. The second cell was positioned so that the PV surface of the second cell contacted the PV surface of the first cell. A foam-covered plate was placed over the assembly and weights were applied to the aluminum plate in order to achieve a particular contact pressure. The top cell was then moved relative to the bottom cell with a displacement of approximately 0.05 inches along the direction of the gridlines for a period of 20 seconds. The process was repeated with the displacement direction perpendicular to the gridlines. The electrical performance of the test cell was then determined. The contact pressure was then increased and the durability test repeated. Three contact pressures (0.1, 0.2 and 0.3 psi) were studied. Two different contact surfaces (PV to PV and PV to ohmic) were evaluated. The durability test matrix is shown in Table 3.

Table 3. Durability Test Matrix

Sample No.	Contacting Surfaces	SiO2 Thickness (μm)	Pressure (psi)	Duration (sec)
1000A1	PV to PV	0.1	0.1, 0.2, 0.3	20/20,20/20,20/20*
1000A2	PV to PV	0.1	0.1, 0.2, 0.3	20/20,20/20,20/20*
1000A3	PV to Ohmic	0.1	0.1, 0.2, 0.3	20/20,20/20,20/20*
1000A4	PV to Ohmic	0.1	0.1, 0.2, 0.3	20/20,20/20,20/20*
10000B1	PV to PV	1.0	0.1, 0.2, 0.3	20/20,20/20,20/20*
10000B2	PV to PV	1.0	0.1, 0.2, 0.3	20/20,20/20,20/20*
10000B3	PV to Ohmic	1.0	0.1, 0.2, 0.3	20/20,20/20,20/20*
10000B4	PV to Ohmic	1.0	0.1, 0.2, 0.3	20/20,20/20,20/20*
30000C1	PV to PV	3.0	0.1, 0.2, 0.3	20/20,20/20,20/20*
30000C2	PV to PV	3.0	0.1, 0.2, 0.3	20/20,20/20,20/20*
30000C3	PV to Ohmic	3.0	0.1, 0.2, 0.3	20/20,20/20,20/20*
30000C4	PV to Ohmic	3.0	0.1, 0.2, 0.3	20/20,20/20,20/20*

* Duration: Test cell in contact with adjacent cell under specified pressure. Test cell moved relative to static adjacent cell (20 seconds along direction of gridlines, 20 seconds across direction of gridlines).

The post-test LAPSS data showed that the cells with the 1.0 μm and 3.0 μm SiO_2 coatings had no measurable degradation in performance following the durability testing at the three contact pressure levels. The cells with the thinnest SiO_2 coating (0.1 μm) showed a significant drop in peak power (10 -11 %). The results of these tests indicated that a 10000A-thick SiO_2 coating to the front surface prevented the cell shunting failure mode caused by direct face-to-face contact as would be seen in a Thin Film UltraFlex application. Even with significant abrasion pressures (well above those expected in an UltraFlex application), damage was limited to minimal power degradation (< 2% reduction in P_{MAX}) in the SiO_2-coated cells. Further tests, including vibration, are planned as part of this study to more thoroughly validate the coatings.

In addition to the protective SiO_2 coating, several interleave options were evaluated in order to protect the cells within the stowed UltraFlex stack. The first interleave option studied was a layer of Tedlar film that rolls up via a lightweight constant force spring as the stowed array stack separates. The roll of interleave film would be located adjacent to the spar when the array was deployed. An engineering model was produced and used to verify the functionality of this interleave concept. This interleave method does add significant complexity to the array deployment.

The second interleave option studied was a static layer of open-weave gore/substrate that covers the front side of the cells. Although this concept is relatively easy to implement, the gore/substrate produces a minimum power loss of approximately 5% over an uncovered cell. The thermal effects of the gore/substrate on array operating temperature need to be evaluated. The SiO_2 coating is the best cell protective option investigated to date.

1.4.6 Large Engineering Gore Circuit

A flight-like engineering gore/blanket circuit of the α-Si FTFPV technology was fabricated that incorporated many of the lessons learned from the previous development/validation tests. A picture of this circuit is shown in

Figure 9. The circuit was laid-down to the UltraFlex substrate/gore and then will be integrated into ABLE's 1st generation IR&D qualification wing, as shown in Figure 10. Wing system level tests will then be performed to further validate the implementation of the α-Si FTFPV technology within the UltraFlex platform.

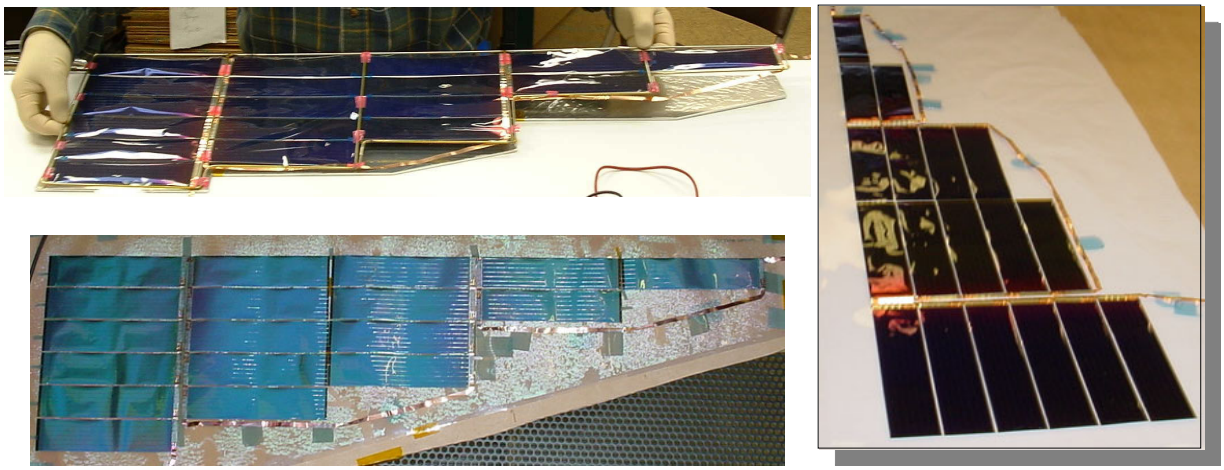

Figure 9. Engineering Gore/Blanket Circuit

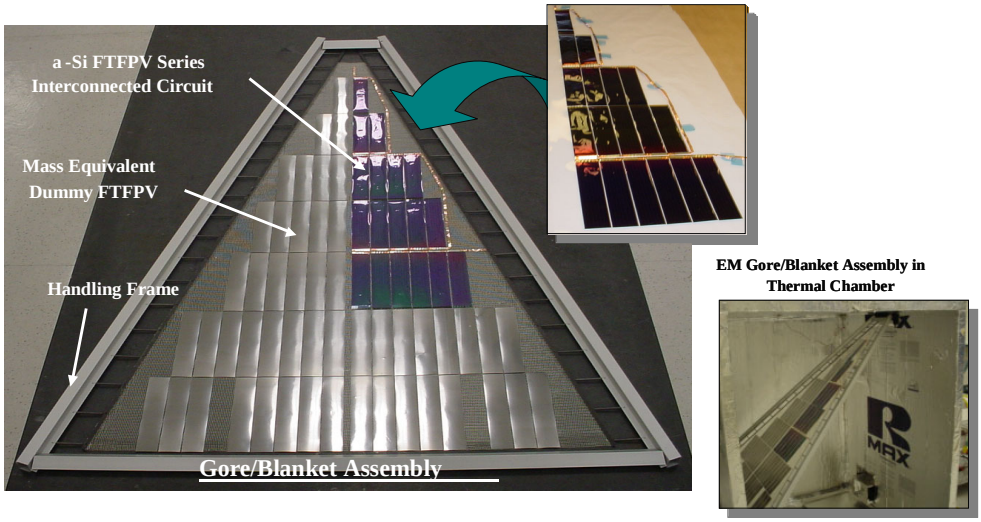

Figure 10. EM Gore Circuit Integrated into Prototype UltraFlex Substrate Gore

The 18-cell USS circuit mounted to the EM gore was coated with 1 μm SiO_2 and 60 nm of ITO. LAPSS tests were performed on the circuit both before and after the coating operation. The preliminary results of the LAPSS tests performed on the circuit after coating indicated a 34% power reduction from the pre-coated circuit, as shown in Figure 11.

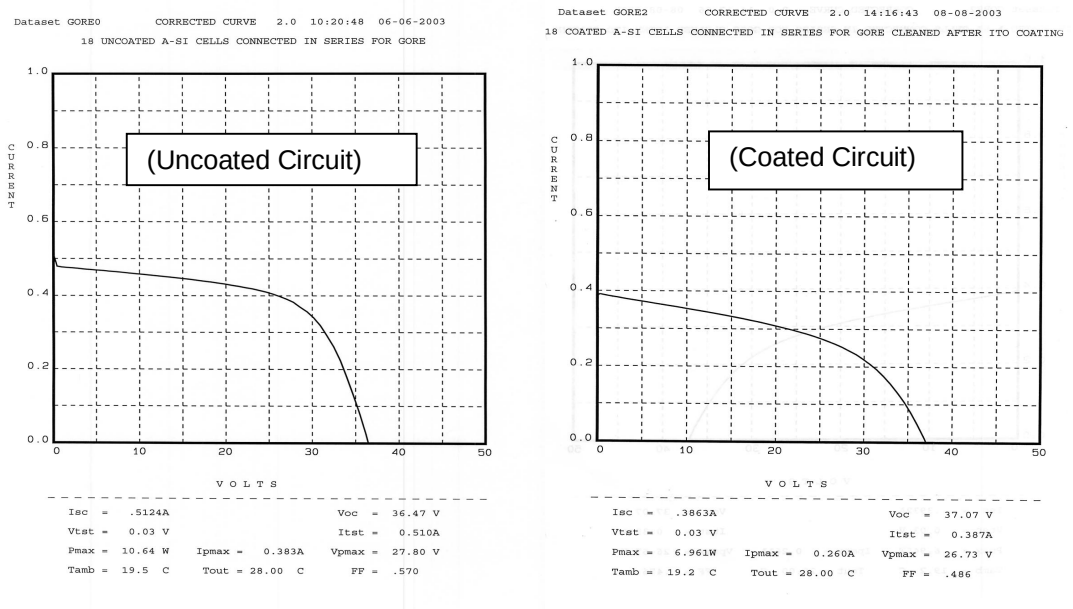

Figure 11. Pre and Post-Coating LAPSS Test Results for 18-cell EM Circuit

Because of the observed degradation in power as a result of the coating, an investigation was initiated to evaluate the cause of the power reduction. The investigation indicated that the shorting between the conductive ITO coating and the cell front photovoltaic surface was occurring through pinholes in the SiO_2. Currently, United Solar is researching suitable front-surface space-rated conductive coatings and application methods to eliminate this problem. Cells to be subsequently tested will be coated with 1 μm SiO_2 only (no ITO).

1.4.7 MISSE Flight Experiment Coupons

Flight experiment coupons of the thin film UltraFlex designs were produced for the Materials of the International Space Station Experiment–5 program (MISSE-5). The purpose of the Materials International Space Station Experiment (MISSE) is to characterize the performance of new prospective aerospace materials when subjected to the effects of the space environment. Two FTFPV UltraFlex flight experiment coupons were produced, each with a different FTFPV technology. The first experiment employed USS α-Si FTFPV, while the second experiment used ITN Energy's CIGS. Both experiments were laid down to a dedicated UltraFlex gore/blanket assembly. The USS α-Si circuit consisted of two AM0 cells with Al/ZnO back reflector on 1-mil stainless steel substrate with single layer side "B" Kapton tape termination. A redundantly welded copper interconnect was used to connect the two cells. Cell to cell interconnection, I-V performance, and operating temperature will be assessed during this experiment. Pictures of the MISSE-5 flight experiment coupons are shown in Figure 12.

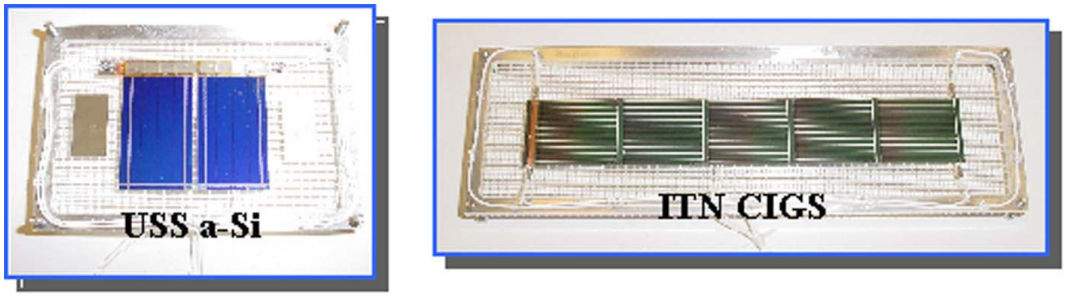

Figure 12. MISSE-5 FTFPV UltraFlex Flight Experiment Coupons

1.5 ACKNOWLEDGMENT

This work was administered though the NASA Glenn Research Center and funded by the NASA SBIR Phase 2 program under contract #NAS3-02078.

1.6 THIN FILM ULTRAFLEX PROGRAM SUMMARY

The initial results of this program indicate that advanced FTFPV can be successfully integrated to a lightweight optimize UltraFlex solar array to produce a system that exhibits very high specific power. This program has provided an important foundation towards validating through hardware development cell-to-cell interconnection, electrical circuitry, circuit laydown and blanket/gore construction, survivability (thermal life cycling and face-to-face contact) and wing/array system level aspects. Future work will involve a series of wing system-level integration and validation activities that will further demonstrate concept feasibility, and more detailed hardware approach to assess face-to-face survivability of the FTFPV under a vibration environment. Additionally, an advanced UltraFlex incorporating the alternative ITN CIGS thin film technology will be developed and validated

2. NASA SBIR PHASE 1 LOW COST/MASS ELECTROSTATICALLY CLEAN SOLAR ARRAY (ESCA) PROGRAM

2.1 INTRODUCTION

Electrostatic interaction of solar arrays in a space plasma environment is of great concern as differential charging across panel portions can lead to high electric fields, charge loss to plasma, and arcing between critical components, which may disrupt scientific measurements of fields or particles [4]. The objective of this program is to develop a low cost and low mass Electrostatically Clean Solar Array (ESCA) which will not interfere with sensitive spacecraft instruments/measurements and ready this technology for commercialization and use on NASA and commercial programs such as the NASA MMS and GED missions. Previous developed ESCA designs are shown in references [5, 6, & 7].

Solar array electrostatic cleanliness is achieved when circuitry is sealed to prevent exchange of charge with the plasma, or unintentionally between cell/string components, and all exterior surfaces are sufficiently conductive to prevent charge differentials on the panels. In meeting this objective, two innovative ESCA solutions have successfully been developed and tested. These are shown in Figure 13 (Zone 1 and Zone 2). The first design uses conductive adhesive grout, which is grounded to the panel core, to electrically connect the ITO coated coverglass on the front of the cells and create an external ground plane. The second design uses conductive tape grounded to the panel core to seal circuitry, electrically connect the ITO coverglass, and create an external ground plane. In both designs, the front-side solar cell circuitry is fully encapsulated in non-conductive adhesive for electrical isolation prior to the application of the conductive exterior ESCA treatment. On the panel backside layers of non-conductive natural Kapton film and conductive polymer films are used for circuit sealing and conductivity. The ESCA designs use flight proven materials and processes to create ESCA systems that yields low cost, low mass, high reliability, high power density, and adaptability to any cell type and coverglass thickness.

2.2 REQUIREMENTS

The NASA requirements and goals specified in Table 4 form the basis of the ESCA design solutions. All requirements and goals shown in Table 4 are met by ABLE's ESCA designs.

2.3 ANALYSIS

2.3.1 Mass Analysis

Mass calculation summaries for the conductive grout and conductive tape ESCA treatments are presented in Table 5. Mass was calculated on a per Cell-Interconnected-Cover (CIC) basis so that the relative magnitude of the mass could be easily determined and so that the calculation would be independent of panel type. The results show that the mass added by either ESCA treatment compared to the CIC's is < 8% and compared to a typical solar panel assembly < 3%, on a per unit area basis. However, the mass of an ESCA solar array also increases by approximately another 10% on a kg/W basis because of the increased panel area required due to the ESCA treatment reducing the total illumination area. The mass of the conductive tape treatment was found to be

significantly lighter than the conductive grout treatment. Both treatments meet the NASA specification for mass increase (<20%).

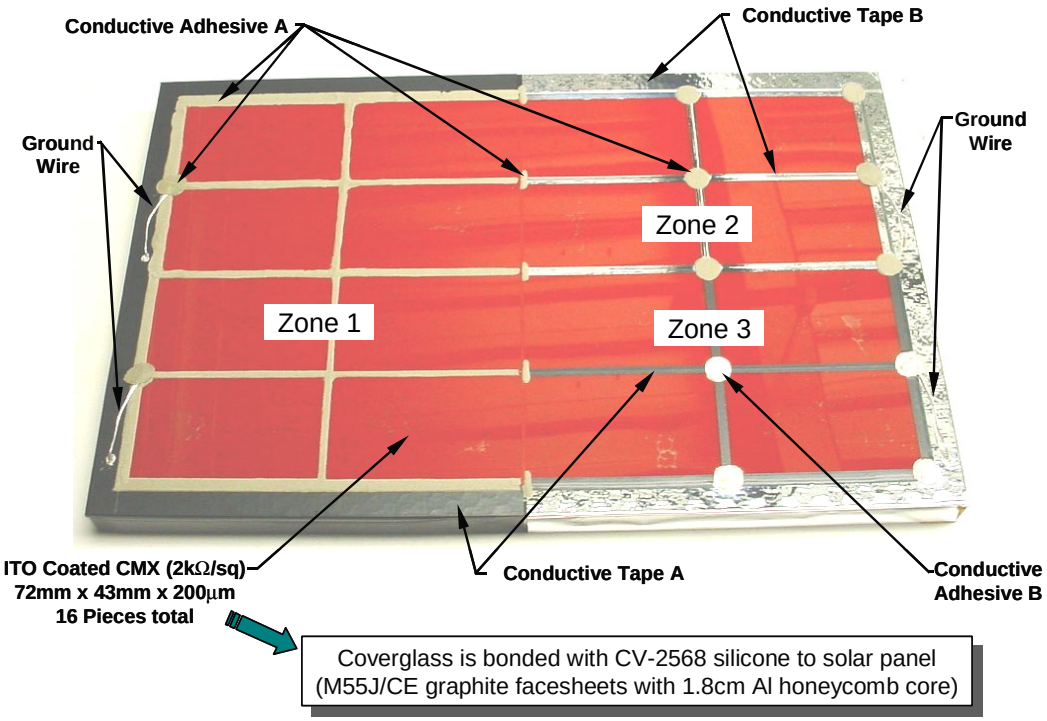

Figure 13. Phase I ESCA demonstration panel that was successfully thermal cycled 2,000 times between -90°C to 100°C (LEO) and 1,350 times from –175°C to 75°C (GEO)

Table 4. NASA ESCA System Requirements/Goals

#	NASA Requirement/Goal Description
1	Regardless of size, there shall be no more than 100 millivolts between any two points on a given panel's surface, even in the presence of a current of 0.1 microampere per square centimeter caused by the ambient plasma
2	The ESCA system shall not induce an electric potential greater than 0.1 volts, at a distance of 0.1 cm or greater from the panel surface, compared with a perfectly conductive surface grounded to the spacecraft structure
3	There shall be no exposed insulator on the panel's front or rear surfaces to the charged particle environment
4	The ESCA system shall be capable of having its quasi-equipotential surface connected to the spacecraft through a connector
5	The proposed method to achieve electrostatic cleanliness shall be compatible with cover thicknesses from .004 inches to .060 inches
6	The proposed method to achieve electrostatic cleanliness shall be compatible with any type of solar cell typically used on spacecraft solar arrays including single crystal silicon, GaAs/Ge, and multi-junction solar cells
7	The ESCA design shall only use materials that exhibit no more than 1.0- percent total mass loss and no more than 0.1 percent-collected volatile condensable materials from outgassing in a vacuum
8	The methods to achieve electrostatic cleanliness shall be compatible with typical spacecraft solar array materials and assembly processes
9	The ESCA design shall use no magnetic parts
10	The ESCA design shall lend itself to easy cell removal and replacement
11	The method to achieve electrostatic cleanliness shall not increase array cost ($/W) by more than 20%
12	The method to achieve electrostatic cleanliness shall not increase array mass (W/kg) by more than 20%
13	The method to achieve electrostatic cleanliness shall not significantly decrease the reliability of the solar array
14	The method to achieve electrostatic cleanliness shall be applicable to multi-AU missions

Table 5. Mass Summary for ESCA Treatments

Mass Calculation Summary for Conductive Grout ESCA Treatment

Cell Length (cm)	3.76
Cell Width (cm)	7.61
Cell-to-Cell Gap (cm)	0.0762
Grout Overlap on Cell (cm)	0.0508
Grout Thickness (cm)	0.0381
Grout Volume per CIC (cc)	0.077
Grout Density (g/cc)	3.4
Grout Mass per CIC (g)	0.262
Measured CIC Mass, 100µm cover (g)	3.34
Grout as a percentage of CIC mass	7.8%
Typical CIC mass fraction of solar panel	36.0%
Deduced grout mass fraction of solar panel	**2.8%**

Mass Calculation Summary for Aluminized Tape ESCA Treatment

Cell Length (cm)	3.76
Cell Width (cm)	7.61
Cell-to-Cell Gap (cm)	0.0762
Tape Overlap on Cell (cm)	0.0508
Tape Thickness (cm)	0.00635
Tape Volume per CIC (cc)	0.013
Tape Average Density (g/cc)	1.4
Tape Mass per CIC (g)	0.018
Conductive Adhesive Corner Dots per CIC (g)	0.055
Total ESCA mass per CIC	0.073
Measured CIC Mass, 100µm cover (g)	3.34
ESCA as a percentage of CIC mass	2.2%
Typical CIC mass fraction of solar panel	36.0%
Deduced ESCA mass fraction of solar panel	**0.8%**

2.3.2 Power Analysis

ESCA treatments reduce power by blocking sunlight that would normally hit the edges of the cell and because ITO coated coverglass has lower transmittance compared to AR coated coverglass. The reduction in transmittance for ITO coated glass compared to standard MgF_2 AR coated glass for the $GaInP_2$ (top) junction of a triple-junction solar cell calculated from the manufacturer's data is shown in Figure 14. The calculated power reduction for the conductive grout and conductive tape ESCA treatments are presented in Table 6. The total power reduction for both treatments is about 8%, of which 5% is due to light blockage and 3% due to reduced transmittance through the ITO. The power reduction can be reduced slightly by using oversize cover glass so that less or none of the cell is blocked by the conductive grout or tape.

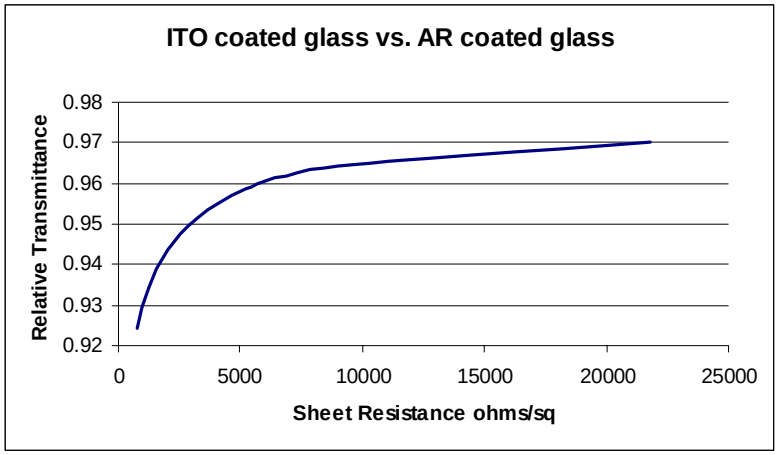

Figure 14. Relative Reduction in Solar Cell Current for ITO Coated Glass

Table 6. Power Reduction for ESCA Treatments

ESCA Power Adjustment Factors Summary
Conductive Grout Treatment

Cell Length (cm)	3.76
Cell Width (cm)	7.61
Cell Area (cm^2)	28.6
Overlap Along Edges (cm)	0.051
Covererd Area (cm^2)	1.14
Average Blocked Light %	4.0%
Cell-to-Cell Variation in Blocked Light %	1.0%
Worse Case Blocked Light %	5.0%
ITO Coverglass Transmittance Loss (%)	3.0%
Total	**8.0%**

ESCA Power Adjustment Factors Summary
Aluminized Kapton Treatment

Cell Length (cm)	3.76
Cell Width (cm)	7.61
Cell Area (cm^2)	28.6
Overlap Along Edges (cm)	0.051
Covererd Area Edges (cm^2)	1.14
Covered Area Dots (cm^2)	0.14
Average Blocked Light %	4.5%
Cell-to-Cell Variation in Blocked Light %	1.0%
Worse Case Blocked Light %	5.5%
ITO Coverglass Transmittance Loss (%)	3.0%
Total	**8.5%**

2.3.3 Cost Analysis

The material cost in both the conductive grout and conductive tape ESCA treatments are relatively low. Most of the cost associated with both methods is due to labor. The estimated recurring cost for the ESCA treatments are presented in Table 7. The treatments are relatively inexpensive comprising only about 5% of the solar panel cost based on an area basis. However, more panel area (~8%) is required to obtain a given power level compared to an untreated panel. Thus, in terms of $/W the increase in cost is approximately (1.05)(1.08) = 1.134. Both ESCA treatments meet the NASA requirement for cost (<20% cost increase). These cost estimates do not include any non-recurring engineering, which would be required for a 1st of a kind array.

Table 7. Estimated Recurring Cost for ESCA Treatments

ESCA Cost Summary
Conductive Grout Treatment

Materials	
CV2-2646 $/Gram	5
Installed Grams/CIC	0.26
Waste Factor	1
Waste (g)	0.26
Total Grams/CIC	0.52
CV2-2646 Cost/CIC	**$2.62**
Labor	
Time Per Task (minutes)	
Inspection	3
Masking	2
Grouting	3
Clean-up	3
Inspection	2
Rework	2
Misc	5
Total Labor (min)	**20**
Assumed Labor Rate $/min	$1.00
Labor Cost per CIC	**$20.00**
Material Cost per CIC	$2.62
ESCA Treatment Total	**$22.62**
Typical 3J CIC Cost	$450.00
ESCA Cost/CIC Cost	**5.0%**

ESCA Cost Summary
Aluminized Tape Treatment

Materials	
Aluminized Kapton ($/$cm^2$)	0.78
Installed Area (cm^2/CIC)	2.02
Waste Factor	1
Waste (cm^2/CIC)	2.02
Total cm^2/CIC	4.04
CV2-2646 Cost/CIC	**$3.15**
Labor	
Time Per Task (minutes)	
Inspection	1
Taping	2
Adhsive Dots	2
Inspection	2
Rework	2
Misc	5
Total Labor (min)	**14**
Assumed Labor Rate $/min	$1.00
Labor Cost per CIC	**$14.00**
Material Cost per CIC	$3.15
ESCA Treatment Total	**$17.15**
Typical 3J CIC Cost	$450.00
ESCA Cost/CIC Cost	**3.8%**

2.4 DEMONSTRATION HARDWARE AND TEST RESULTS

Based on the results of pathfinder coupon tests, the Phase 1 ESCA engineering model, shown in Figure 15, was fabricated using the most promising conductive adhesive and conductive tape treatments. T he engineering model contained sixteen pieces of ITO coated coverglass (72mm x 43mm x 200microns). The engineering model was thermal cycled 2,000 times in a LEO environment and 1,350 times in a GEO environment. Visual inspections and resistance measurements were made prior to and after thermal cycling. The visual inspection results and resistance measurements are shown in Figures 16. The conductive adhesive (zone 1) and conductive tape B (zone 2) passed both the mechanical and electrical test criteria. The conductive tape A treatment (zone 3) failed both mechanically and electrically.

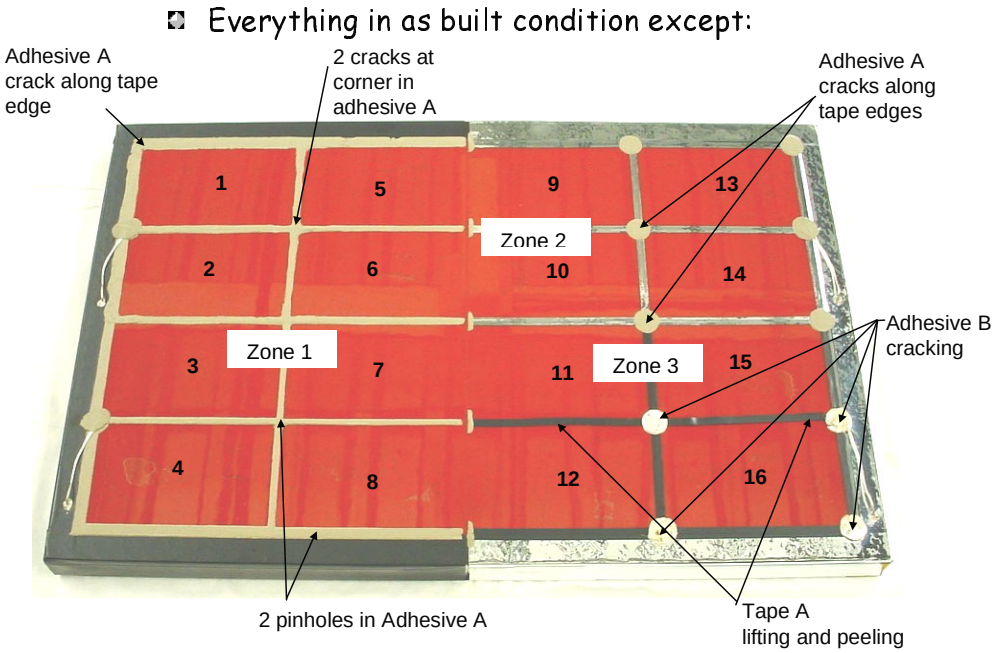

Figure 15. Visual Inspection Results for Engineering Model After 2,000 LEO Cycles and 1,350 GEO Cylces Between –175°C and 75°C

Glass	Treatment	Ground Resistance (kΩ)*		Comment
		Pre Test	Post Test	
1	Conductive Adhesive	1.0	1.1	Pass Mechanical and Electrical
2	Conductive Adhesive	1.5	1.6	Pass Mechanical and Electrical
3	Conductive Adhesive	1.5	1.2	Pass Mechanical and Electrical
4	Conductive Adhesive	1.5	1.3	Pass Mechanical and Electrical
5	Conductive Adhesive	1.0	1.0	Pass Mechanical and Electrical
6	Conductive Adhesive	2.2	1.5	Pass Mechanical and Electrical
7	Conductive Adhesive	3.0	1.2	Pass Mechanical and Electrical
8	Conductive Adhesive	1.4	1.1	Pass Mechanical and Electrical
9	Conductive Tape B	1.6	1.8	Pass Mechanical and Electrical
10	Conductive Tape B	1.6	2.7	Pass Mechanical and Electrical
13	Conductive Tape B	2.3	2.4	Pass Mechanical and Electrical
14	Conductive Tape B	6.3	8.5	Pass Mechanical and Electrical
11	Conductive Tape A	2.0	1.8	Fail, Tape Peeling, Adhesive Cracking
12	Conductive Tape A	2.0	3.3	Fail, Tape Peeling, Adhesive Cracking
15	Conductive Tape A	2.6	3.8	Fail, Tape Peeling, Adhesive Cracking
16	Conductive Tape A	6.0	OVLD	Fail, Tape Peeling, Adhesive Cracking

*Less than 30kohm required to meet ESCA requirement of 0.1V maximum
2,000 LEO Thermal Cycle from -90°C to +100°C
1,350 GEO Thermal Cycles from -175°C to +75°C

Figure 16. Coverglass Ground Resistance Results for Engineering Model After 2,000 LEO Cycles and 1,350 GEO GEO Cylces.

2.5 ELECTRICALLY ACTIVE ESCA PANEL

An electrically active engineering model of the conductive tape ESCA treatment containing nine TECSTAR TEC1 3J solar cells (Donated by EMCORE) wired in series was fabricated and is shown in Figure 17. The power of the electrically active engineering model was measured before and after application of the ESCA treatments to measure the effect on power. The results, which are shown in Figure 18 show a decrease in current (Isc) of 4.6% and a decrease in power (P_{max}) of 6.3% which is in good agreement with the predicted light blockage of 5.5% calculated in Table 6.

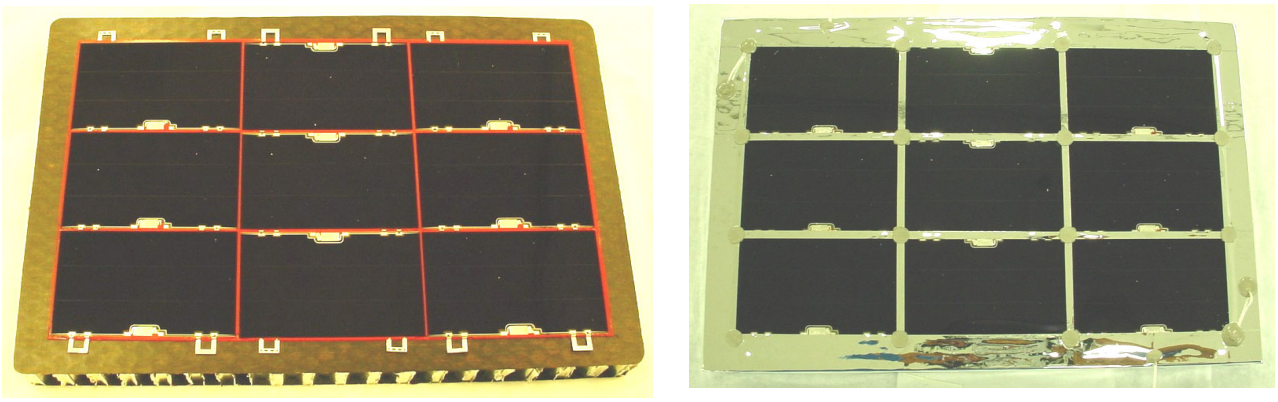

Figure 17. Electrically Active Prototype Before and After ESCA Treatment

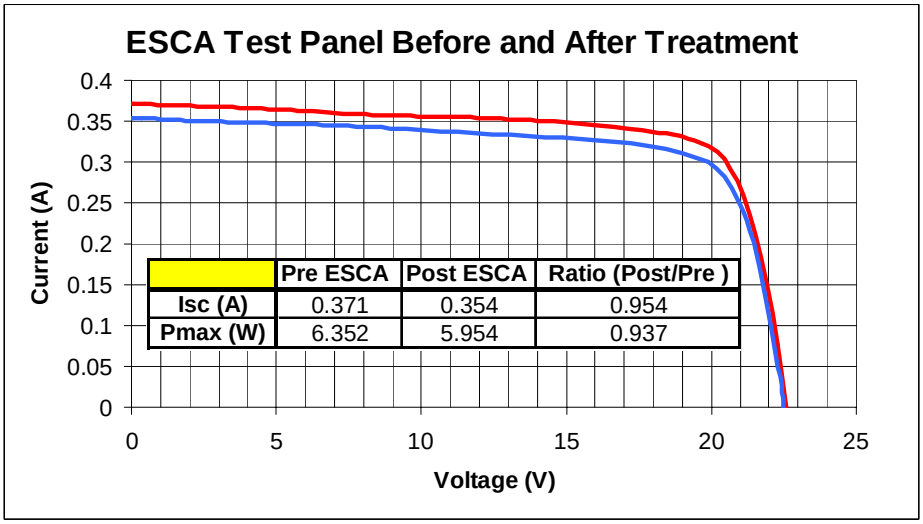

Figure 18. LAPSS Results for Active ESCA Test Panel

2.6 ACKNOWLEDGMENT

This work was administered though the NASA Goddard Space Flight Center and funded by the NASA SBIR Phase 1 program under contract #NAS5-03030.

2.7 ESCA SUMMARY

Electrostatically Clean Solar Array (ESCA) technologies meeting NASA's design requirements have been developed in preparation for commercialization and use on the NASA MMS and GED missions. The ESCA designs developed use flight proven materials and processes to create ESCA systems that yields low cost, low mass, high reliability, high power density, and is adaptable to any cell type and coverglass thickness. All Phase 1

objectives, which included developing specifications, creating ESCA concepts, concept analysis and trade studies, producing detailed designs of the most promising ESCA treatments, manufacturing ESCA demonstration panels and LEO (2,000 cycles) and GEO (1,350 cycles) thermal cycling testing of the down-selected designs were successfully achieved. It is hoped that these exceptional Phase 1 results and the high payoff of this technology to NASA GSFC's planned MMS and GED missions result in a Phase 2 continuation of this program.

3. NASA PHASE 1 SBIR HIGH POWER PLATFORM FOR THE STRETCHED LENS ARRAY

3.1 INTRODUCTION

The purpose of this program is to develop an extremely lightweight, high efficiency, high power, high voltage, and low stowed volume solar array suitable for very high power (multi-kW to MW) applications. This is achieved by integrating a Stretched Lens Array (SLA) blanket into the SquareRigger (SR) solar array structure. The resulting solar array is termed Stretched Lens Array SquareRigger (SLASR).

SLASR uses SquareRigger, which is a well demonstrated structural approach for deploying extremely large photovoltaic blankets in terms of low mass, low stowed volume, and high stiffness and the SLA Fresnel concentrator, which is believed to be the best-demonstrated photovoltaic system in terms of the desirable combination of low cost, high efficiency (30%), ultra-low mass (>500 W/kg blanket), and high voltage (>1000V). The proposed SLA concentrator elements are highly optimized versions of the extremely successful Deep Space 1 SCARLET solar array lenses [8]. An electrically active, flight-like, SLASR demonstration blanket was successfully fabricated and tested during Phase 1 and is shown in Figure 19. The excellent optical alignment achieved by the prototype SLASR blanket is shown in Figure 19 where the focus of natural sunlight on to the solar cells is demonstrated by the gossamer structure.

The predicted near-term (<5 years) BOL performance for a 100 kW SLA SquareRigger array system is a specific power of 320 W/kg, a power per unit area of 310 W/m^2, and a stowed power per unit volume of 70 kW/m^3 *using the existing designs and demonstrated triple-junction solar cell technology*. These characteristics of the SLA SquareRigger solar array, which are based on detailed models, make it an ideal candidate for meeting civil, military and commercial future power generation needs.

Figure 19. SLASR Demonstration Blanket Built During Phase 1
(Precise Optical Alignment of Prototype SLASR Demonstrated in Sunlight)

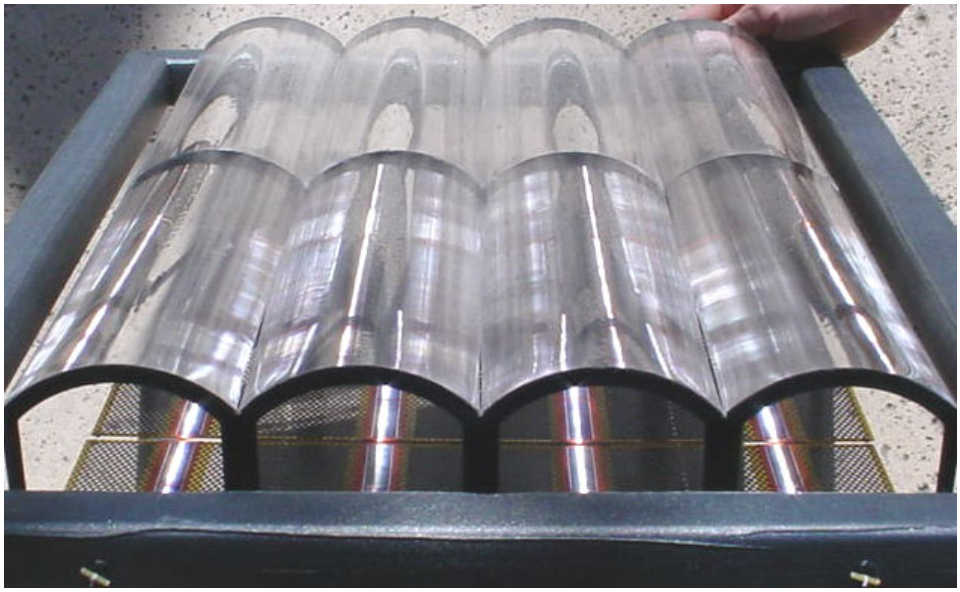

3.2 BACKGROUND

The SquareRigger solar array structure (Figure 20) was developed by ABLE for the Air Force Research Laboratory (AFRL) to deploy and structurally support very large thin film solar array blankets for future high power Air Force missions. The key features of SquareRigger (using a hypothetical 0.2 kg/m^2 thin film photovoltaic blanket made from 15% efficient CIGS) are very high power capability, low cost ($/W), low mass (>200 W/kg), and compact stowage for launch (>40 kW/m^3) [1]. These highly desirable characteristics may also enable numerous future NASA missions including Space Solar Power (SSP), high-power deep space SEP probes, Solar Electric Propulsion (SEP) tugs and large earth-orbiting science satellites.

While the SquareRigger structure development has progressed rapidly, with all elements of 2nd generation hardware recently demonstrated at full scale as shown in Figure 21, the high efficiency (>15% AM0 & 0.2 kg/m^2) thin film photovoltaic blanket needed to complete this extremely lightweight, low cost, and high power solar array is currently not available. Additionally, there are many experts in the photovoltaic community who are concerned that the timeframe to develop a space-qualified, high efficiency, thin film blanket may be much longer than currently projected and that the attained performance will be lower than anticipated and the cost higher than expected. Thus, it is very desirable to develop alternative low cost and low mass photovoltaic blanket technologies for SquareRigger in case thin film photovoltaics are unavailable when needed. It is also highly desirable to develop a much more efficient photovoltaic system compared to thin films to greatly reduce the deployed area and the launch volume of the SquareRigger array. The Stretched Lens Array (SLA) blanket, under development for SquareRigger in this program, fits these requirements perfectly.

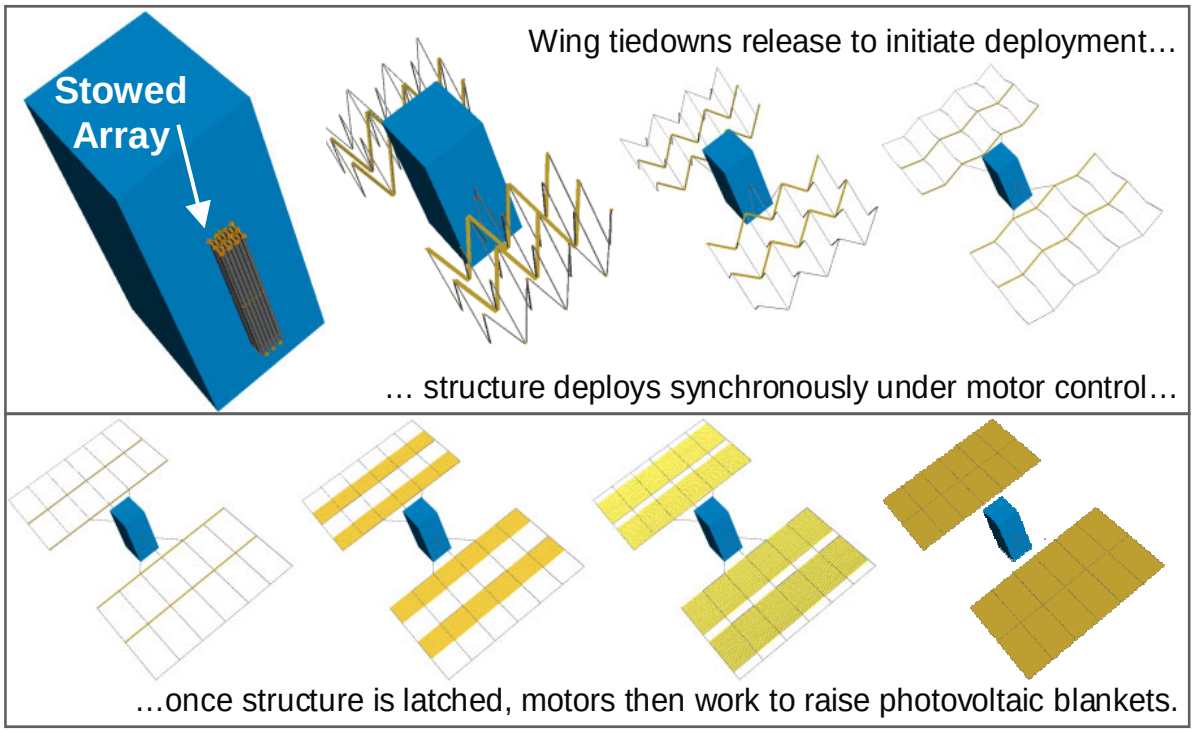

Figure 20. SquareRigger Structure and Blanket Deployment

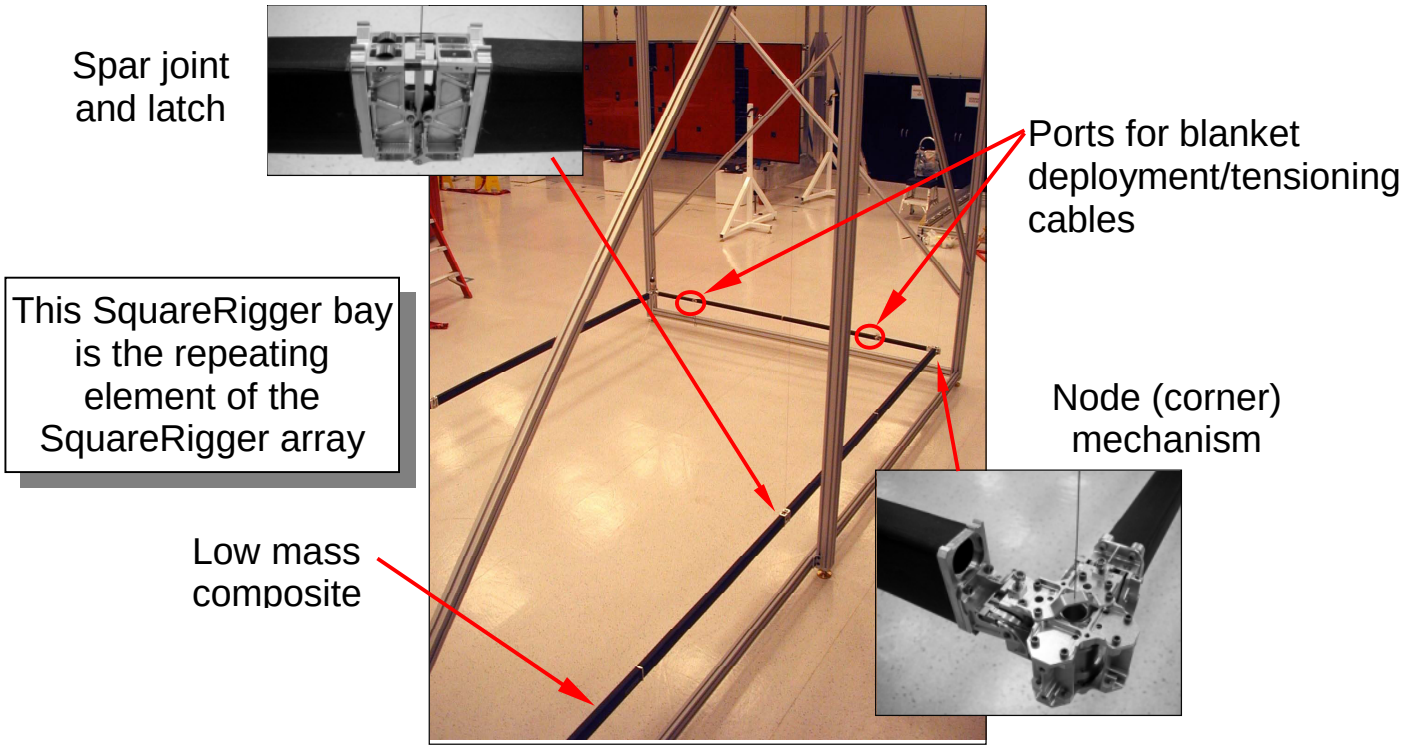

Figure 21. Full-Scale SquareRigger Bay after Successful Ground Deployment

The Stretched Lens Array (SLA) [9] is a low mass/low cost *high efficiency* photovoltaic system that uses gossamer line-focus Fresnel lenses to focus sunlight at approximately 8.5X concentration on to spaced rows of high performance crystalline solar cells. The current embodiment of SLA on optimized rigid panels is well suited for lower power level spacecraft, offering a robust 180 W/kg, but not as well suited as SLA SquareRigger for high power applications (>15 kW wings). This is because SquareRigger was developed to specifically to overcome scale-up problems inherent in rigid panel platforms and provide lower mass and stowed volume.

The SquareRigger platform can accommodate nearly any photovoltaic blanket technology. The AFRL is leading the development of thin films for space applications and the SquareRigger is a leading structural platform candidate. ABLE recently completed an AFRL funded program developing a thin film SquareRigger solar array system and also a crystalline (standard multi-junction cell) blanket as a backup technology to thin films, as this offers lower risk in the near term but much higher cost and mass. Alternatively, SLA technology adapted to SquareRigger simultaneously provides small deployed wing area and stowed volume (due to the use of high efficiency multi-junction cells), and low cost and low mass (enabled by a 70% to 80% reduction in cell area) approaching/surpassing the best thin film projections.

Typical components of a SLA blanket, which can directly replace the thin film solar cell blanket in SquareRigger, are shown in Figure 22. The early version of the SLA photovoltaic blanket, also shown in Figure 22, was developed as part of the SSP program for use in a lower performing, earlier generation, “Space Station” style blanket array platform known as Aurora. Though built in 2000, this fully functional demonstration blanket was measured by NASA Glenn Research Center to have an output of greater than 375 W/m^2 at 20°C equating to a lens efficiency of 92%, a cell efficiency of 30.0%, and over 400 W/kg [4]. The SLA blanket developed for SquareRigger is an optimized version of this early concept.

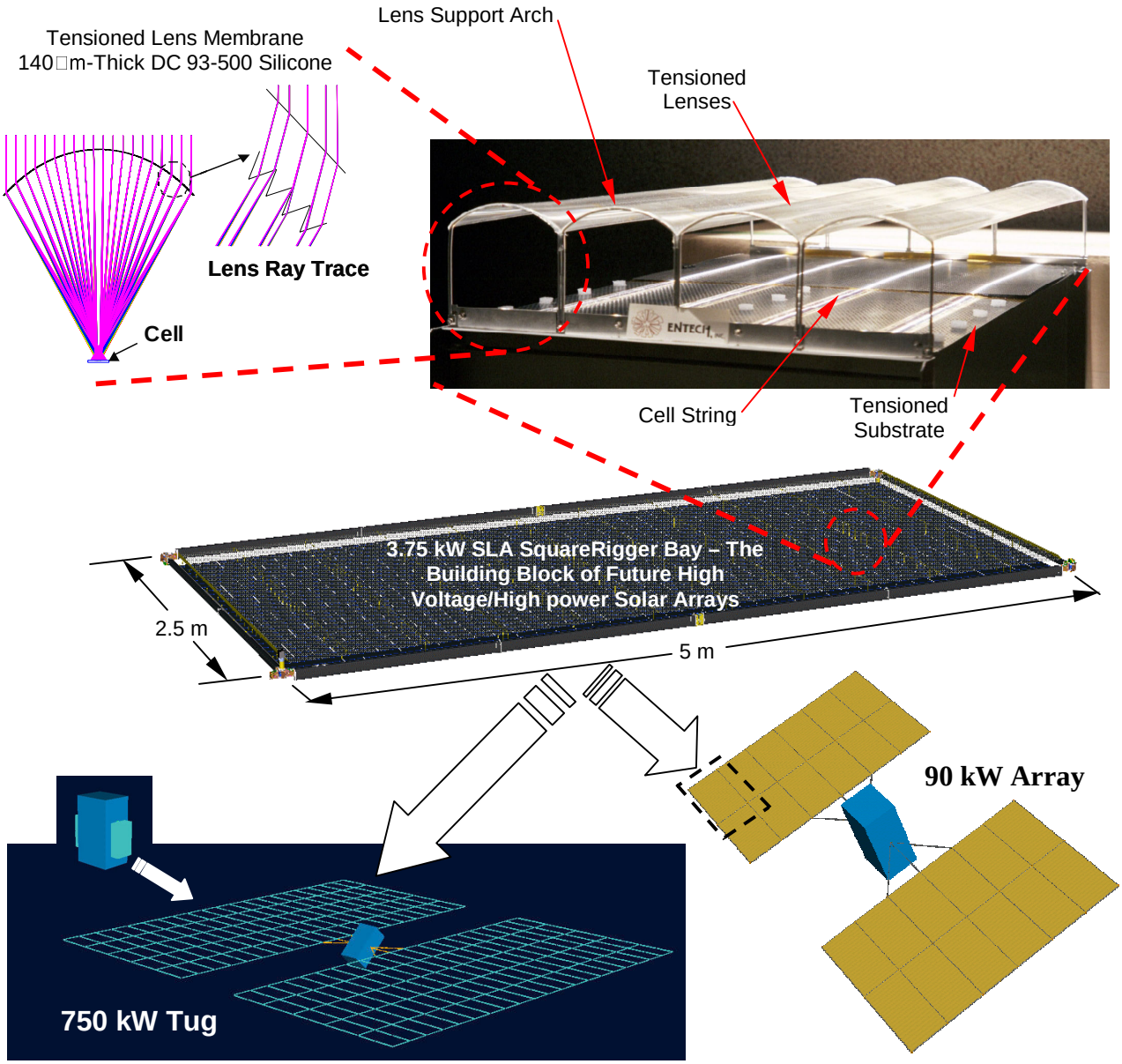

Figure 22. Stretched Lens SquareRigger (SLASR) Array

3.3 SLASR System Requirements and Goals

At the start of the Phase 1 program requirements/goals were developed for SLASR for both the near-term (2008) and mid-term (2013). These requirements, which are shown in Table 8, specify the performance metrics for the system (e.g. W/kg, W/m2, $/W etc.) and also define the launch and on-orbit environmental durability. These performance metrics were aggressively set to vastly improve the state of art in cost, mass, and stowed power density. The environmental durability requirements are representative of typical space solar array industry requirements and are based on ABLE's broad experience in manufacturing solar arrays for commercial, NASA and military missions. These requirements were reviewed by NASA personnel and modified as required based on NASA's input. All detailed design, analysis and testing performed during Phase 1 support the attainment (or very near) of all the requirements/goals as is shown in later sections. For the cases where projected performance, based on Phase 1 results, is now slightly less than the original goals it is shown in parenthesis.

Technical specifications specific to the SLA blanket were then derived from the system requirements and the structural characteristics and capabilities of SquareRigger. These blanket specifications, which are shown in Table 9, were used as the design guideline for the SLA blanket during Phase 1.

Table 8. Original Requirements/Goals Developed for SLA SquareRigger System

Characteristic	When?	Near-Term Requirement (2008)	Mid-Term Requirement (2013)
Missions		LEO, MEO, GEO & Interplanetary	
Deployed Power (kW)	EOL	10 to 100	
Stowed Power (kW)	BOL	0	
Recurring Production Cost ($/ W)	BOL	250	125 (150)
Specific Mass (W/kg)	BOL	330 (320)	500
Deployed Power Density (W/m^2)	BOL	300	390
Stowed Volume (kW/m^3)	BOL	80 (70)	120 (110)
Voltage (V)	EOL	100 to 1000	
Radiation Degradation (e^-, p^+, UV)	EOL	Comparable to multi-junction planar array	
Contamination Degradation	EOL	Comparable to multi-junction planar array	
Thermal Cycling Degradation	EOL	Comparable to multi-junction planar array	
Micrometeoroid Degradation	EOL	Comparable to multi-junction planar array	
Quasi Static Acceleration	Launch	22 g's in each axis	
Acoustic Vibration	Launch	146 dB OASPL for 120 seconds	
Stowed Stiffness (fn Hz)	Launch	> 30 Hz	
Deployed Stiffness (fn Hz)	On-Orbit	> 0.1 Hz for 10kW , > 0.01 Hz for 100kW	
Deployed Accelerations	On-Orbit	0.001g's	
Grounding, ESD	On-Orbit	No sustained arcs or degradation, minimize trigger arcs	
System Reliability	EOL	0.99	
Deployment Torque Margin	On-Orbit	200% (3 to 1)	
Deployment Time	On-Orbit	1 hour total, 30 min structure, 30 min blanket	
Ground Test Capability	Pre-Launch	LAPSS test at the bay level (5m x 2.5m section)	
Assumed Cell Efficiency (8AM0, 28°C)	BOL	30%	40%
Pointing Accuracy at Base	On-Orbit	+/- 1 degrees	

3.4 SLASR BLANKET DESIGN

The primary components of the dual-deck lens and cell panel blanket are shown in Figures 23, 24, 25, and 26. The ultra-thin Fresnel lenses used in the dual-deck SLA blanket, which are made of electron, proton, and UV radiation resistant DC 93-500 silicone, are 0.14-µm-thick and are spaced approximately 9 cm from the solar cells. The flexible lenses are tensioned over arches, with approximately one meter of span of lens between arches, to produce a curved shape that significantly increases shape-error tolerance and off-pointing performance compared to flat Fresnel lenses. The solar cells are mounted to thin (130micron or less) graphite-composite panels optimized for high stiffness and efficient waste heat removal via high thermal conductivity and emissivity. Both the lens film and composite panels are tensioned end-to-end between the struts of the SquareRigger structure when the array is deployed. The demonstrated tension to achieve precise lens shape and alignment is only 1.1 Newton (0.25 lbf) per lens.

Lateral lens-to-cell alignment is critical. Very accurate alignment is achieved by attaching the lens guides and panels to small diameter Kevlar cords tensioned straight between spreader bars, which are attached to the SquareRigger end struts. These primary support cords run continuously between the end interfaces under moderate tension and, therefore, form a near perfect datum for aligning the lens guides and panels. The support cord also doubles as the hinges between panels.

Table 9. Derived Technical Specification the for SLA SquareRigger Blanket

Characteristic	When?	Blanket Specification
Deployed Dimensions		2.54 m wide x 5.08 m long (100 in x 200 in)
Stowed Dimensions	Launch	13.2 cm x 3.3 cm x 2.54 m (5.27 in x 1.35 in x 100 in)
Power	BOL	3.75 kW (290 W/m^2)
Mass		8.25 kg maximum (0.64 kg/m^2)
Operational Voltage	EOL	100 V to 1000 V
Deployed Lens- to-Cell Spacing	On-Orbit	9.22 ± 0.05 cm (3.63 ± 0.02 in) from top of lens arch to face of cell
Deployed Tension (Radiator + Lens)	On-Orbit	44.5 N (10lb) Maximum
Deployment Force	On-Orbit	66.8 N (15lb) Maximum
Cell-to-cell centerline alignment (all cells)	On-Orbit	± 0.025 cm (± 0.010 in) = 0.16 degrees error
Cell-to-lens centerline alignment (all cells)	BOL	± 0.050 cm (± 0.020 in) = 0.31 degrees error
Radiation Degradation (e^-, p^+, UV)	EOL	Comparable to multi-junction planar array
Contamination Degradation	EOL	Comparable to multi-junction planar array
Thermal Cycling Degradation	EOL	Comparable to multi-junction planar array
Micrometeoroid Degradation	EOL	Comparable to multi-junction planar array
Quasi Static Acceleration	Launch	22 g's in each axis
Acoustic Vibration	Launch	146 dB OASPL for 120 seconds
Grounding, ESD	On-Orbit	No sustained arcs or degradation, minimize trigger arcs
Storage	Ground	Meets all requirements after 1 year of stowage (20±5°C, <50%RH)
Deployment Time	On-Orbit	< 30 minutes
Assumed Cell Efficiency (8AM0, 28°C)	BOL	30%
Required Pointing Accuracy (α)	On-Orbit	+/- 1.5 degrees
Required Pointing Accuracy (β)	On-Orbit	+/- 10 degrees

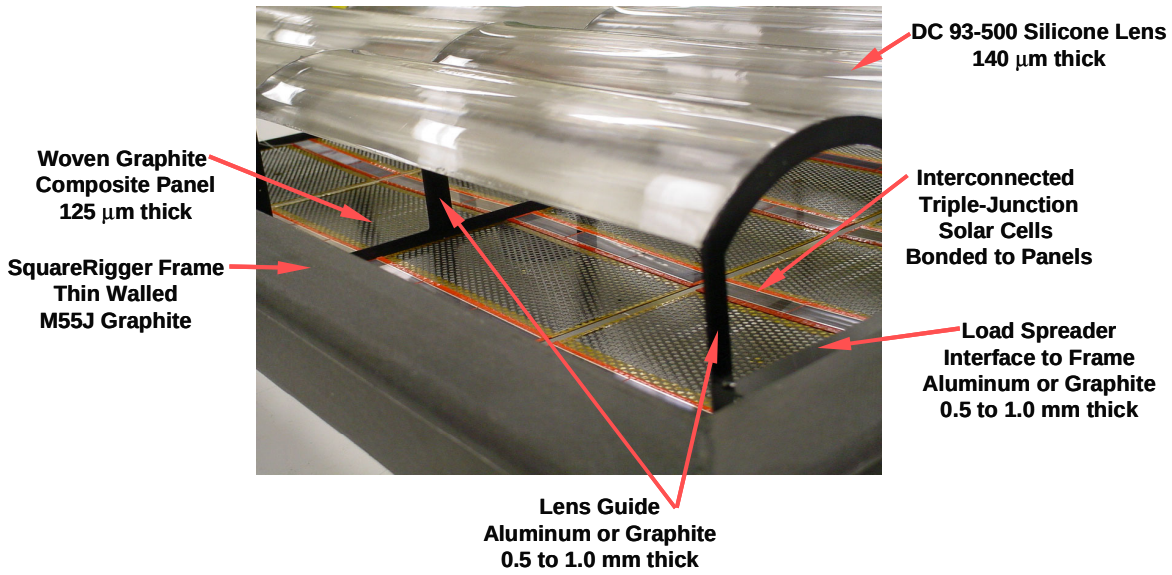

Figure 23. Lens Blanket Components Shown on the Phase 1 Demonstrator

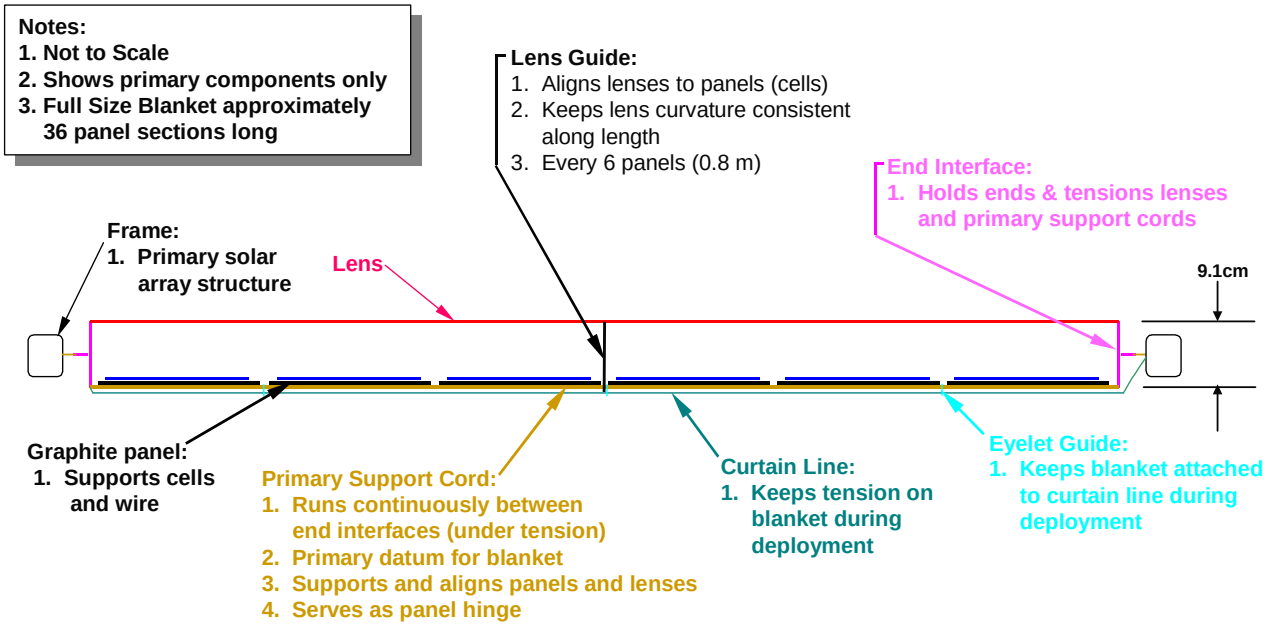

Figure 24. SLA SquareRigger Blanket Primary Components

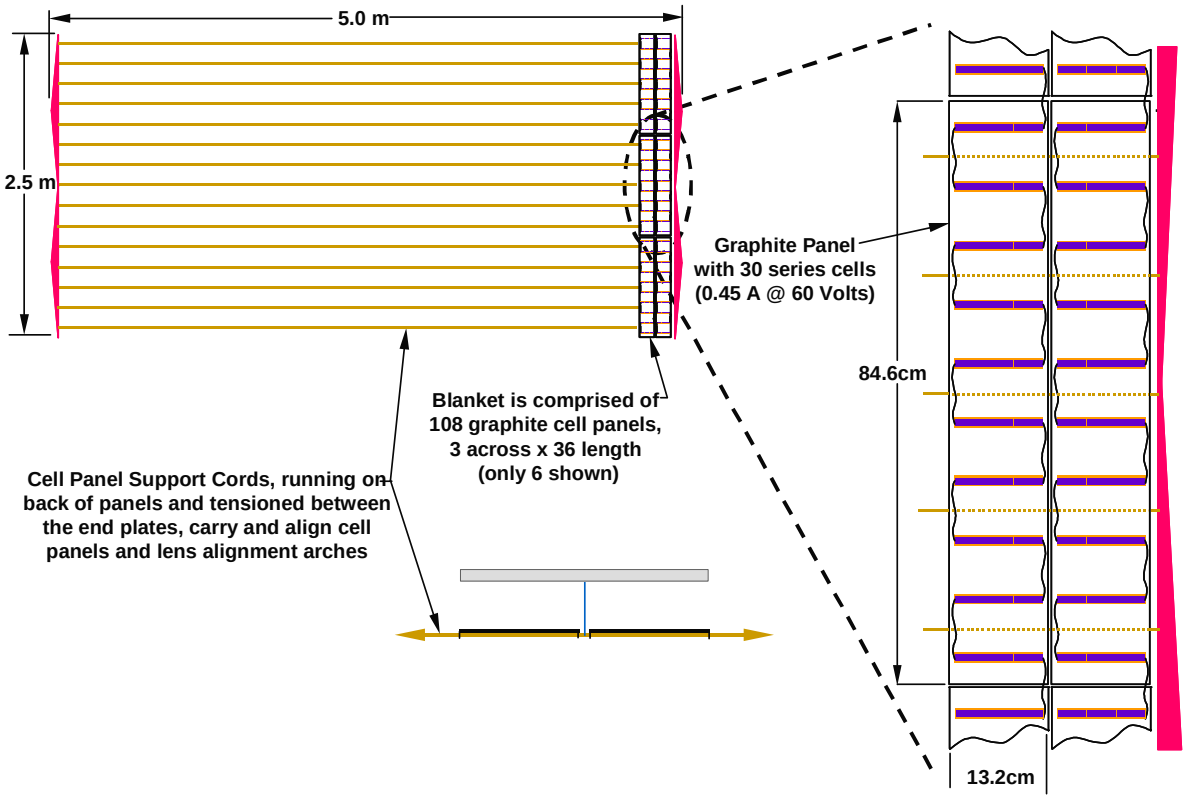

Figure 25. SLA SquareRigger Cell Panel Blanket

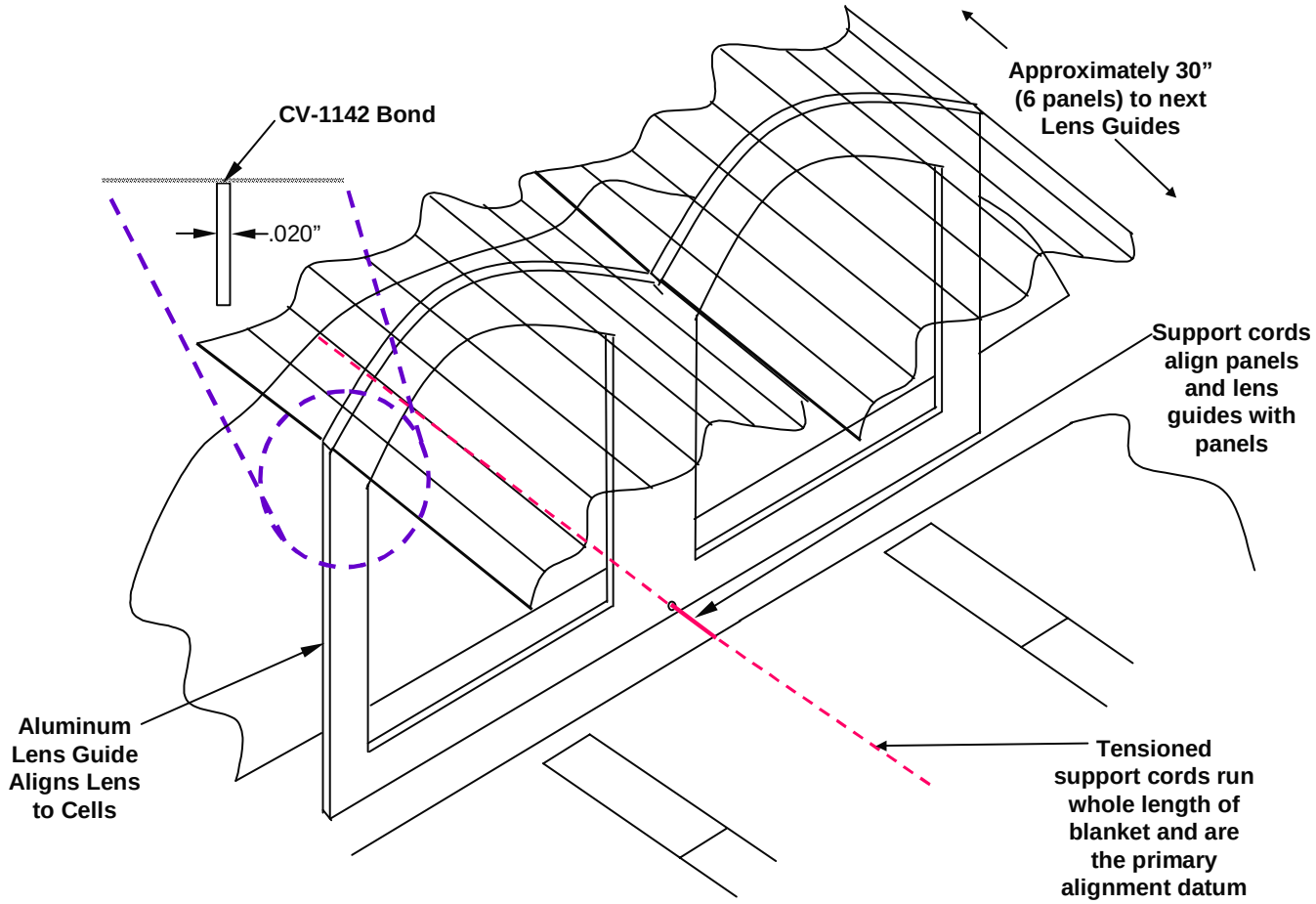

Figure 26. Lens Guide Alignment

A typical deployment sequence for SLA SquareRigger is shown in Figure 27. During launch the dual-deck lens and cell blanket is stowed in a compressed stack in the cavity that exists between the SquareRigger struts and spars to protect them from vibration damage. As shown in Figure 28 and Table 10, the lenses are folded between the cell panels when stowed providing a compact blanket stack, 5.65cm (2.23 in.) tall, which is highly damped. The folded panels and lenses are deployed accordion style pulled by the same motor that unfolded the SquareRigger structural elements. Low spring rate tensioners are used to attach the lens/cell panel blanket to the SquareRigger frame to minimize the effect of thermally induced length change on lens and/or panel tension and to enhance structural stability. These designs for SLA blanket stowage and deployment are derived from the original thin film blanket stowage and deployment concepts.

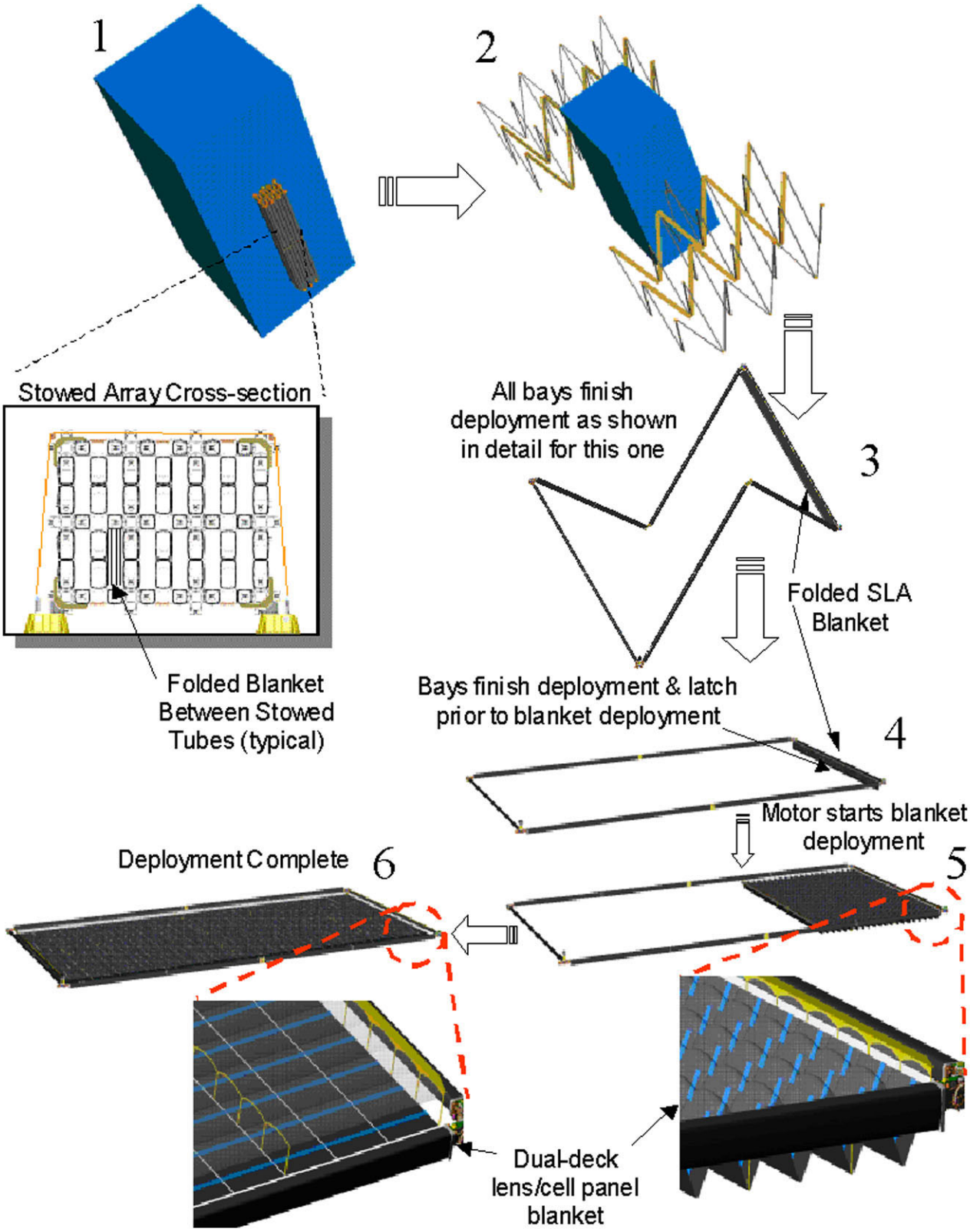

Figure 27. SLASR Stowage and Deployment

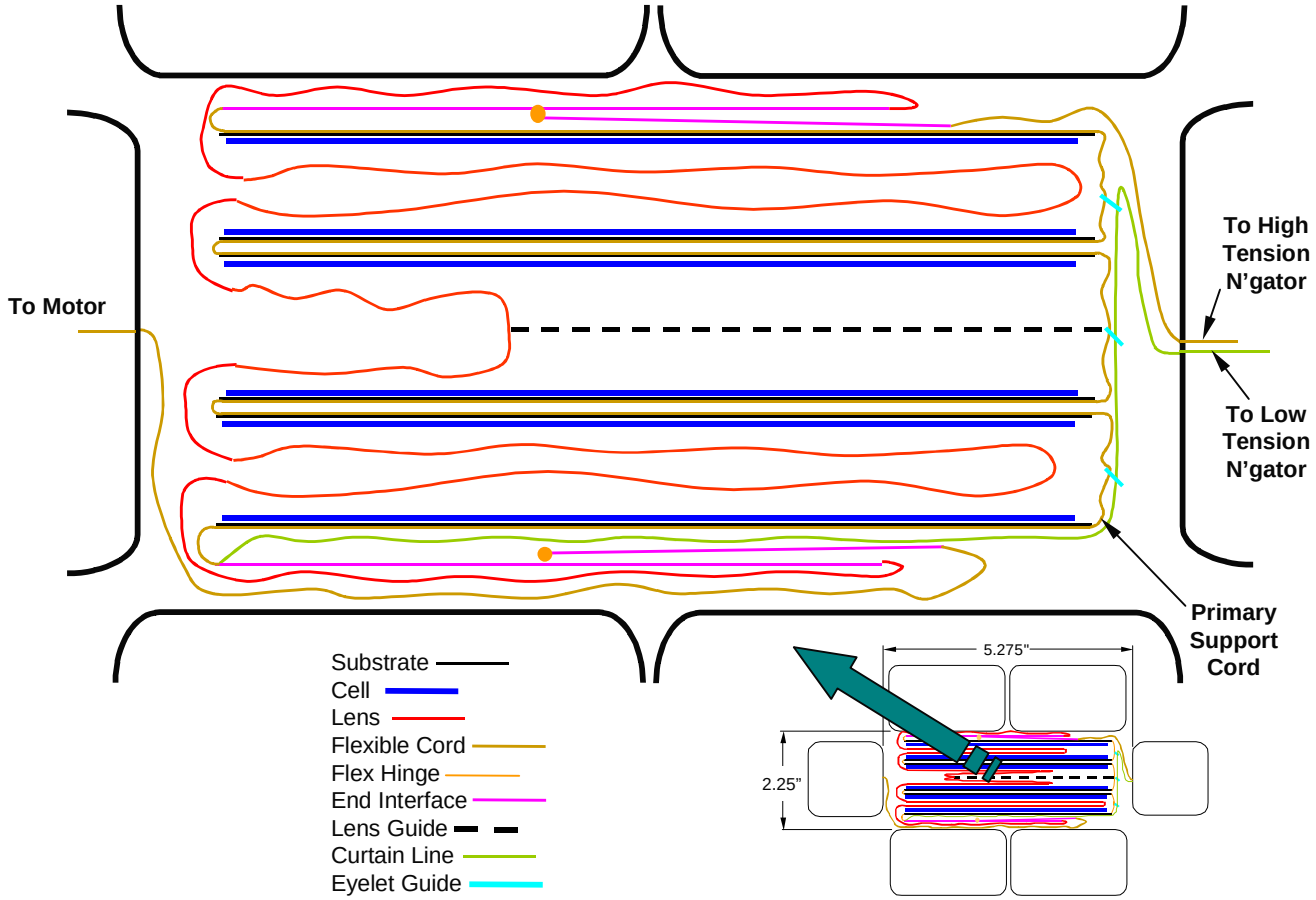

Figure 28. SLASR Blanket Stowage

Table 10. Stowed Blanket Thickness Calcuation

Stowed Blanket Thickness (Inches)				
Component	**Thickness**	**Quantity**	**Total**	**Fraction**
1/2 Cords on Back	0.005	36	0.180	8.9%
Substrate	0.005	36	0.180	8.9%
Flex Bond	0.000	36	0.000	0.0%
Flex Circuit	0.004	36	0.144	7.1%
Cell Bond	0.004	36	0.144	7.1%
Cell	0.006	36	0.216	10.7%
Glass Bond	0.002	36	0.072	3.6%
Glass	0.003	36	0.108	5.3%
Lens	0.008	36	0.288	14.2%
1/2 Lens Fold	0.012	36	0.432	21.3%
Sub Total	0.044	36	1.764	
End Interface Plate	0.04	4	0.160	7.9%
Lens Guide	0.02	5	0.100	4.9%
Nominal Total			**2.024**	**100%**
Contingency			**0.2024**	**10%**
Total with Contingency			**2.226**	

3.5 SYSTEM ANALYSES

3.5.1 Sizing Model

Development of an Excel spreadsheet to rapidly size and predict all key SLASR metrics was completed during the Phase 1 program. The model allows an analyst to quickly and accurately predict SLASR array size, power and mass for any reasonable configuration of bay size, quantity and arrangement. The model contains 22 detailed worksheets addressing the various details of the design such as mass properties, strength, stiffness, power, environmental degradation and packaging in a single Excel file.

The model performs a detailed power analysis. On-Orbit EOL electrical performance is calculated from:

- Measured BOL cell performance
- Detailed radiation dose calculation
- Operating temperature
- Harness Losses
- On-orbit degradation
- Radiation, contamination, UV, micrometeorites, thermal cycling etc.

The detailed mass analysis is based on prototype SquareRigger and SLA hardware as available. The model contains a complete parts list and there is a mass breakout and contingency for each component based on its maturity. Harness mass is determined by wire count and length. A mass contingency, which is currently running at about 5% at the system level, is included in all reported metrics and is calculated for each component based on the following criteria:

- 2% for actual or PRO/E designed part
- 10% for calculated
- 15% for estimated

The model also includes approximate structure strength and stiffness calculations to ensure that these very important features are consistent with the stated requirements. The key metrics of mass (W/kg) and stowed power (kw/m^3) calculated from the sizing model for already demonstrated 30% efficient concentrator cell efficiency is shown in Figure 28. A typical mass breakdown is also shown in Figure 29. A summary of a typical power analysis performed for a high power 15 year GEO mission is shown in Figure 30.

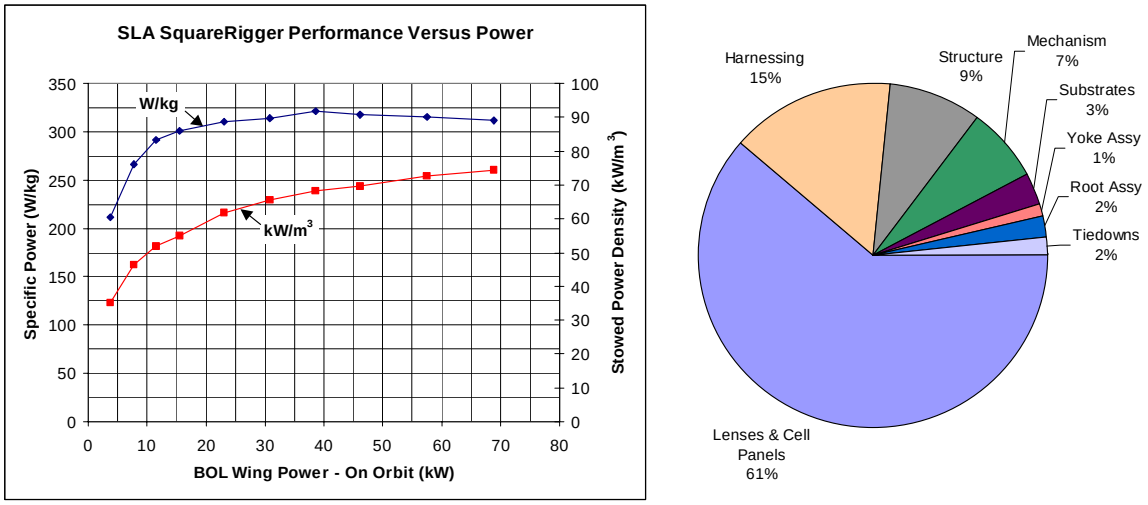

Figure 29. Calculated SLASR Mass and Stowed Power Density and Typcical Mass Breakdown

SLA Triple Junction Cell Data at 1 AM0 and 28 °C	Isc	Imp	Vmp	Voc	Pmp	Efficiency
	Amps/cm^2		Volts			
Bare Cell Performance, BOL 28 °C	0.0177	0.0170	2.389	2.714	0.0406	30.00%
Temperature Coeffcients °C^{-1}	1.00E-05	7.00E-06	-0.0065	-0.0059	-9.37E-05	-0.0693%

15yr GEO Mission

Cell Length (cm)	3.50
Cell Active Width (cm)	1.00
Lens Width (cm)	8.50
Geometric Concentration Ratio	8.50
Lens Gap or Blocking at Edges (cm)	0.076
Lens Optical Efficiency	0.92
Effective Optical Concentration Ratio	7.68
Net Optical Efficiency	0.904
Effective Cell Area (cm^2)	26.88
Concentration Voltage Boost Factor	1.09

	Reference Value	Loss Factor	Isc	Imp	Vmp	Voc	Pmp	System Efficiency
Cell Under Lens @ 28°C			0.476	0.457	2.604	2.958	1.19	29.54%
LAPSS Calibration to AM0		1.000	0.476	0.457				
CIC Assembly Voltage Loss		0.995			2.591	2.943		
CIC Glassing Loss		0.995	0.473	0.454				
Sun Distance	1.0000 AU	1.000	0.473	0.454				
Alpha Off-Pointing		1.000	0.473	0.454				
Beta Pointing (Cosine)	3.00 deg	0.999	0.473	0.454				
Beta Pointing (Shadowing)		1.000	0.473	0.454				
UV degradation, Lens		0.980	0.463	0.445				
UV degradation, Cell Cover		0.980	0.454	0.436				
Micro-Meteoroid and Debris		0.990	0.449	0.432				
Contamination on Lens and Cell		0.980	0.440	0.423				
Isc Radiation Degradation	4.20E+14 1MeVe/sqcm	0.990	0.436					
Imp Radiation Degradation	5.20E+14 1MeVe/sqcm	0.978		0.414				
Vmp Radiation Degradation	5.20E+14 1MeVe/sqcm	0.899			2.330			
Voc Radiation Degradation	5.93E+14 1MeVe/sqcm	0.897				2.639		
CIC Operating Temperature	85.6°C							
Isc Temperature Correction	10.0 uA/sqcm/C	0.0155 A	0.451					
Imp Temperature Correction	7.0 uA/sqcm/C	0.0108 A		0.425				
Vmp Temperature Correction	-6.5 mV/°C	-0.3744 V			1.956			
Voc Temperature Correction	-5.9 mV/°C	-0.3398 V				2.299		
Cell-to-Cell Interconnect Voltage Drop	0.01 ohms	-0.0042 V			1.952			
EOL CIC Performance			0.451	0.425	1.956	2.299	0.83	20.63%
Series Cells Per Module	4	4	0.451	0.425	7.824	9.196		
Module-Module IC Voltage Drop	0.01 ohms	-0.0042 V			7.819			
Cell Module Performance			0.451	0.425	7.819	9.196	3.32	20.62%
Thermal Cycle Current Loss		0.995	0.449	0.422				
Thermal Cycle Voltage Loss		0.995			7.780	9.150		
Cell/Module Stringing Mismatch		0.99		0.418				
Lens Stringing Mismatch		0.99		0.414				
Number of Series Modules per String		15			116.704	137.256		
String Performance on Panel			0.449	0.414	116.704	137.256	48.32	20.01%
Blocking Diode Voltage Drop		0.7000 V			116.004			
Panel Harness Voltage Drop	0.28 ohms	0.1139 V			115.891			
Strings per Power Circuit	**6**							
Wing Harness Voltage Drop	0.95 ohms	2.3563 V			113.534			
String Performance at SADA/Spacecraft Connector			0.449	0.414	113.534	137.256	47.01	19.46%

Input to Array IV curve calculator

Number of Strings = 1188

Voc	Isc	Vmp	Imp	Pmp	FF
137.26	533.60	113.53	491.87	55843.7	0.76

Performance at Load Voltage

Volts	Amps	Watts
100.00	514.07	51406.7
110.00	**503.48**	**55382.3**
113.53	491.87	55843.7

Power at Selected Load Points

Peak Power

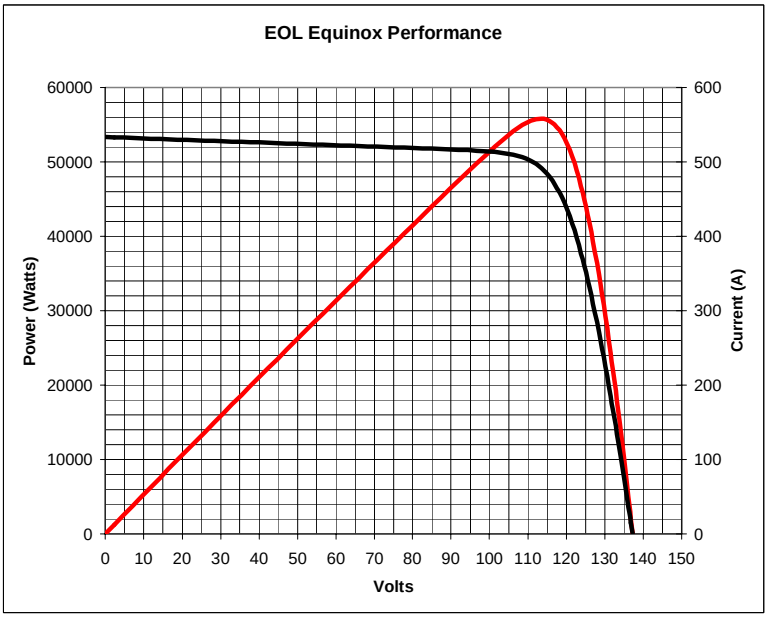

Figure 30. SLASR EOL Power Analysis Example for 56kW 15-year GEO Mission

3.5.2 Detailed Structural Analysis

ANSYS Finite Element models were developed for 14 kW, 42 kW and 56 kW wings to calculate natural frequency and deflection due to acceleration. It was determined that the baseline SquareRigger structure (tube cross-section and thickness), originally developed to support a thin film photovoltaic blanket, meets the SLASR stiffness requirements (frequency > 0.1 Hz for 10 kW Array - 2 Wings, frequency > 0.01 Hz for 100 kW Array - 2 Wings, and maximum a rotation < 1 Degree @ 0.01 g). Results of the finite element calculations are shown in Figure 31.

3.6 MID-TERM (10 YEAR) TECHNOLOGY ROADMAP

All near-term analysis and performance projections are based on the existing designs and current technology capabilities, the most important of which is cell efficiency. Thus, a SLASR array constructed from existing components will achieve the near-term performance given in Table 11. Over the next ten years significant improvements are forecast for many key SLASR technologies. For example *mass produced* crystalline solar cells for space have achieved an average improvement of approximately 1% per year between 1995 (19% SJ GaAs) and 2003 (27.5% ATJ $GaInP_2$/GaAs/Ge) based on the production of over 1.5 million cells and this trend is expected to continue. The key improvements in SLASR technology are listed in Table 11 along with the corresponding impact on the key metrics of efficiency (W/m^2), cost ($/W), mass (W/kg) and stowed power density (kW/m^3).

Table 11. Mid-Term (10 year) Technology Roadmap for SLASR

				Improvement			
Component Improvement	**Current Performance**	**Projected Performance**	**Basis**	**W/m^2**	**W/kg**	**$/W**	**kW/m^3**
Cell Efficiency	30% Efficiency	40% Efficiency	EMCORE and SPL Technology Roadmap Trends	1.33	1.33	1.33	1.33
Solar Cell Module Mass	2.51 grams (4cells)	1.51 grams (4 cells)	Use 1/2 thickness cell being developed by EMCORE. Interconnect Cells without copper flex circuit. Co-cure kapton to panel.	1.00	1.09	1.00	1.05
Lens Mass & Cost	140 μm thick	115 μm thick	Improved processing and materials	1.00	1.03	1.10	1.02
Panel Mass	100 μm thick	75 μm thick	Higher conductivity graphite fibers including carbon nanotubes	1.00	1.05	1.00	1.02
Mechanism Mass		75% reduction from current	Design and material optimization	1.00	1.02	1.05	1.00
Structural Size & Mass		75% reduction from current	Higher modulus graphite fibers including carbon nanotubes	1.00	1.02	1.10	1.10
			Total Improvement Factor	1.33	1.64	1.69	1.60
			Current Performance	300	320	250	70
			10 Year Performance	**400**	**523**	**148**	**112**

3.7 DEMONSTRATION HARDWARE AND TESTING

Based on the full scale SLASR design concepts developed, detailed drawings for the Phase 1 SLA SquareRigger prototype were prepared. As shown in Figures 32 through 35, the demonstration blanket contains four 12.7cm (5.0") x 34.0cm (13.4") woven graphite panels, four approximately 53.3cm (21")-long lenses that are supported by a lightweight graphite SquareRigger frame. The lenses were manufactured and bonded to the aluminum lens guides by ENTECH. The lens and cell panel blankets are tensioned to approximately 4.5 Newtons (1lbf) each and this equates to approximately 4% stretch of the lenses. Left over (scrap) two-junction $GainP_2$/GaAs/Ge TECSTAR cells from the DS1 SCARLET program were installed on the panels to enhance the quality of the demonstrator. Two strings, of 3 cells in series, were installed and interconnected on one of the panels for electrical performance testing. The optical alignment and flatness of the prototype was exceptional as proven by the ease at which all cells can be simultaneously brought into focus as shown in Figure 36.

The blanket deployment concept was successfully verified by manually tensioning the blanket draw cords simulating tensioning of the cords by an electric motor as shown in Figure 37. The power production of the two 3-cell strings was measured using ABLE's Large Area Pulsed Solar Simulator (LAPSS) with and without the lenses installed to record system efficiency. The data from string 1 is shown in Figure 38. The increase in power and current from the lenses was as expected with a measured lens efficiency of 90%. The power and current increase for string 2 was similar to string 1, though it was noted that one of the cells in the strings was damaged, resulting in string 2 having low voltage compared to string 1.

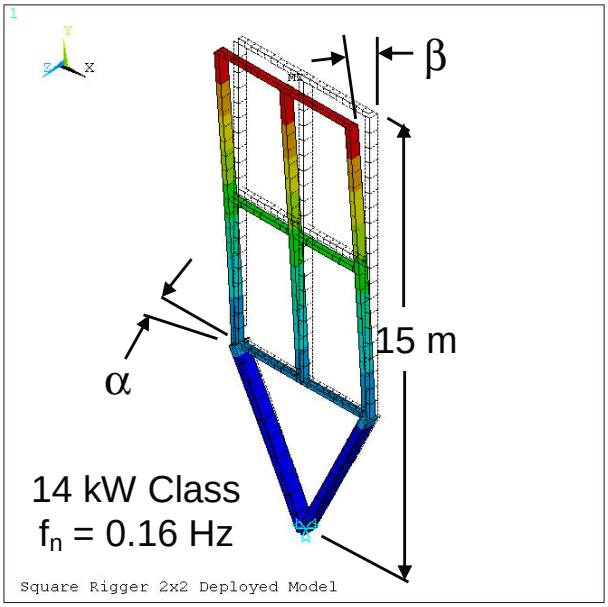

Maximum Rotation at 0.01 g
α = 0.11 deg
β = 0.79 deg

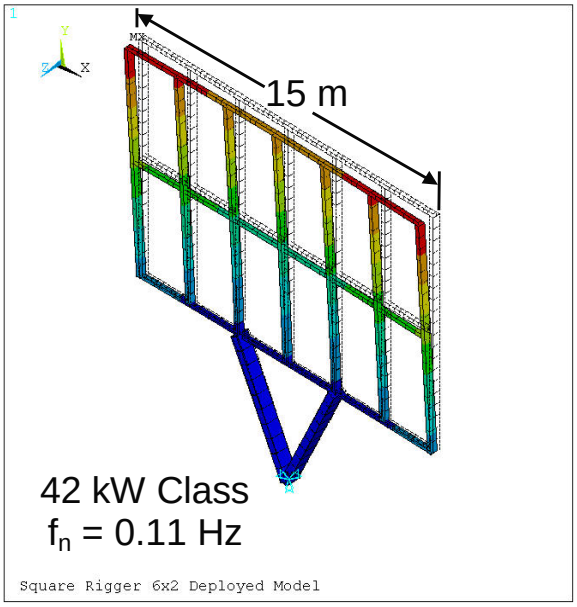

Maximum Rotation at 0.01 g
α = 0.57 deg
β = 1.43 deg

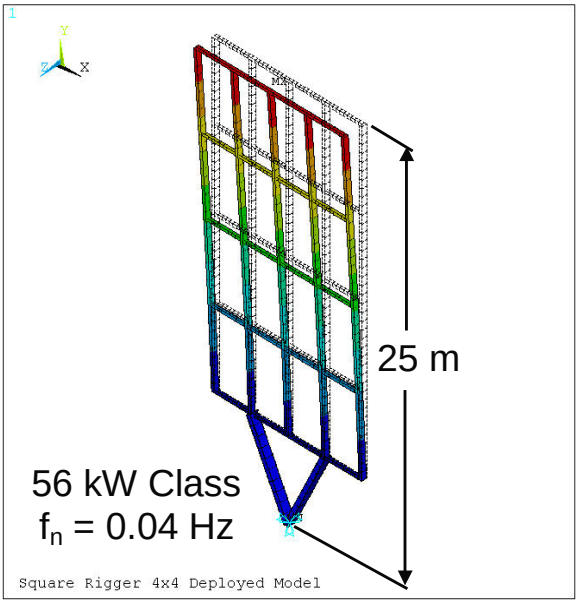

Maximum Rotation at 0.01 g
α = 0.64 deg
β = 5.69 deg

Requirements

- Frequency > 0.1 Hz (10 kW Array= 2 Wings)
- Frequency > 0.01 Hz (100 kW Array = 2 Wings)
- Maximum a rotation < 1 Degree @ 0.01 g

Figure 31. SLASR FEA Stiffness Calculations for Several Configurations Showing Compliance to Requirements

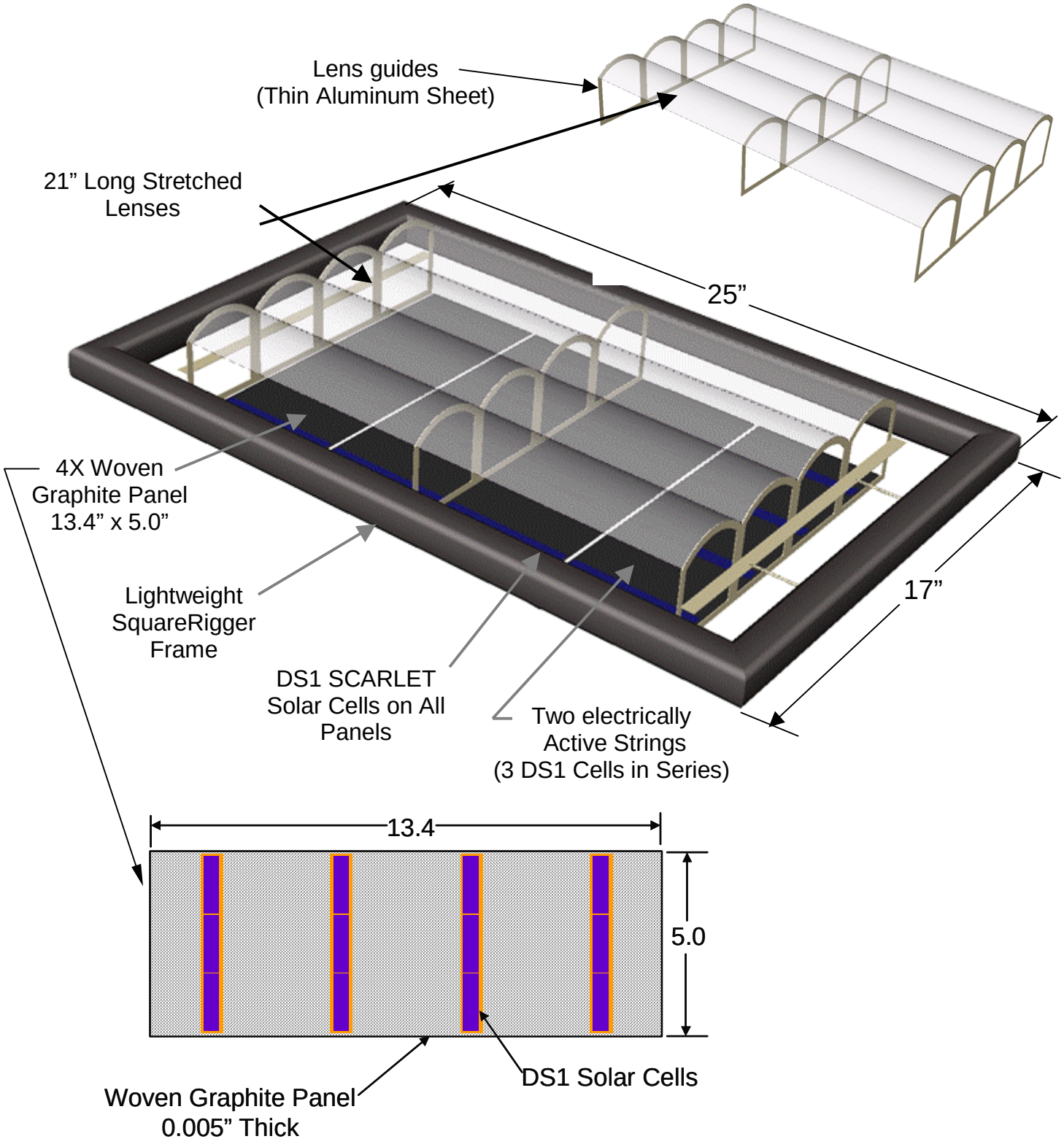

Figure 32. SLA SquareRigger Demonstration Blanket Components

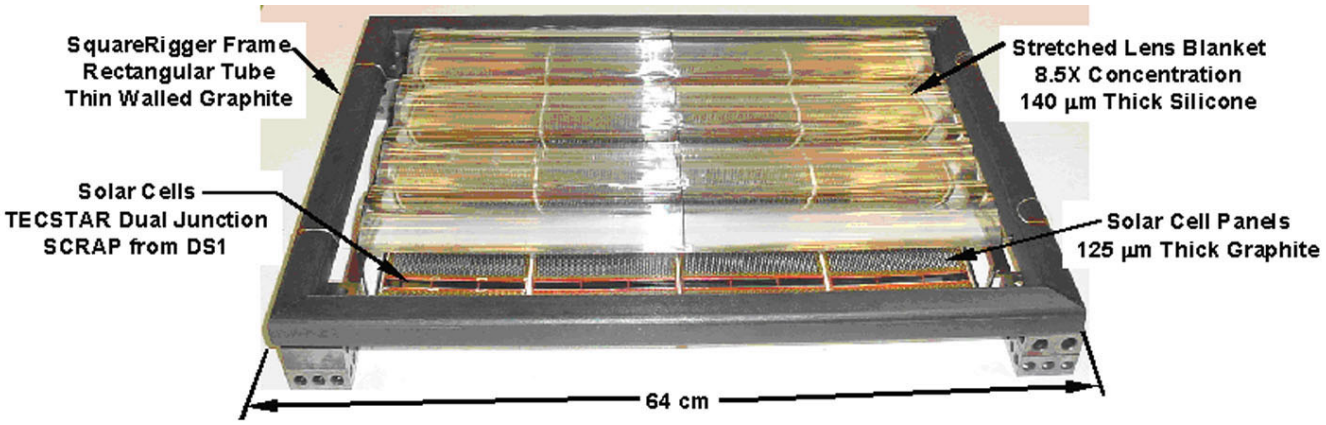

Figure 33. Phase 1 SLASR Prototype Top View

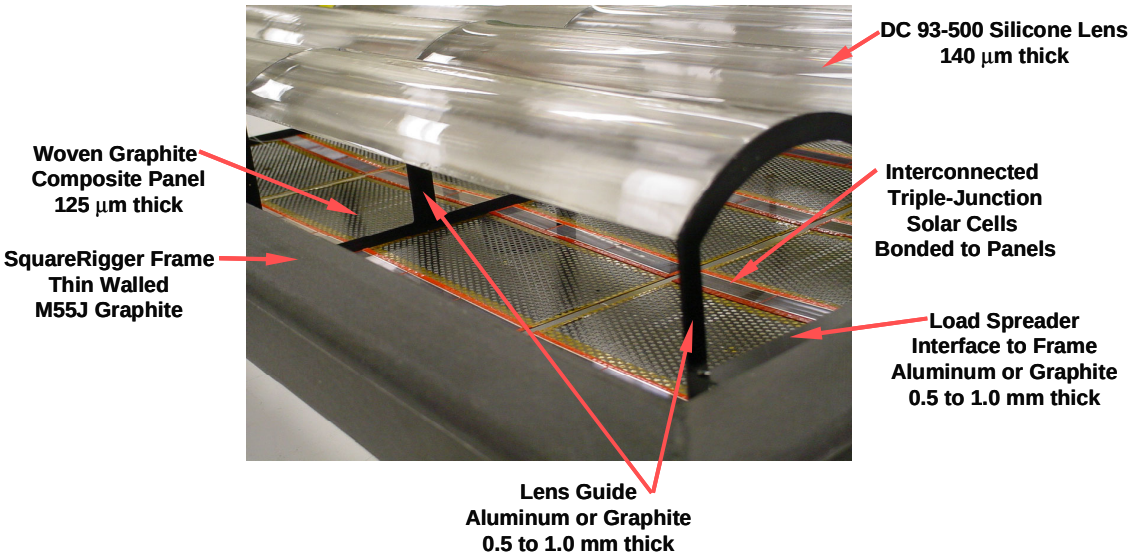

Figure 34. Phase 1 SLASR Prototype Oblique View

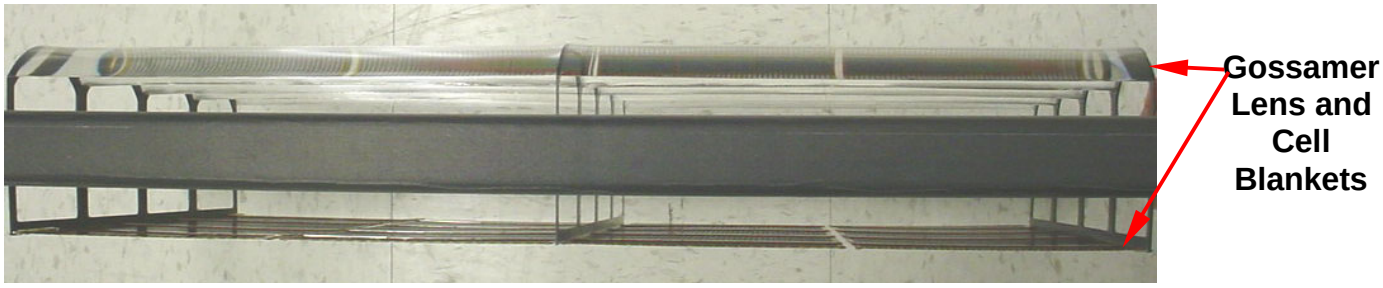

Figure 35. Phase 1 SLASR Prototype Side View

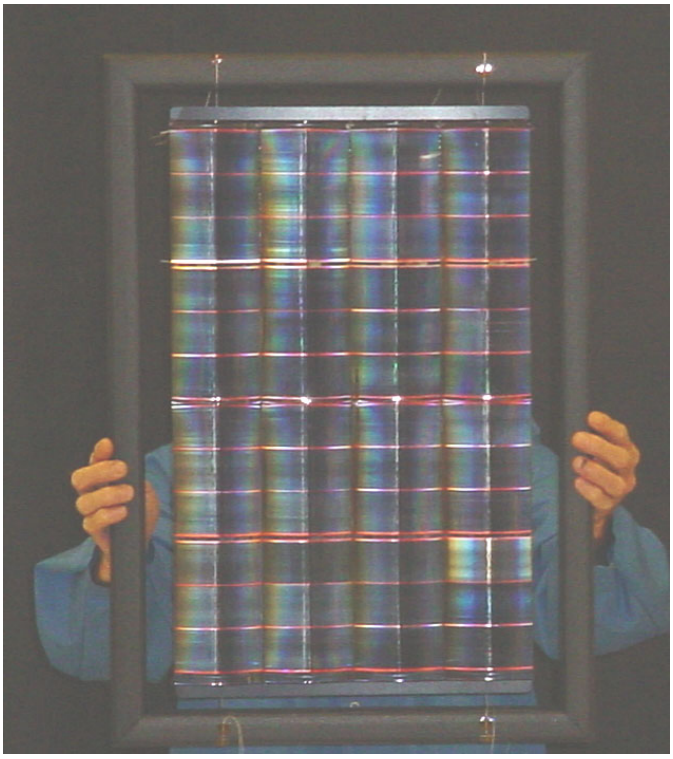

Lenses perfectly image cells verifying optical alignment and flatness

Lenses perfectly focus sunlight on cells verifying optical alignment and flatness

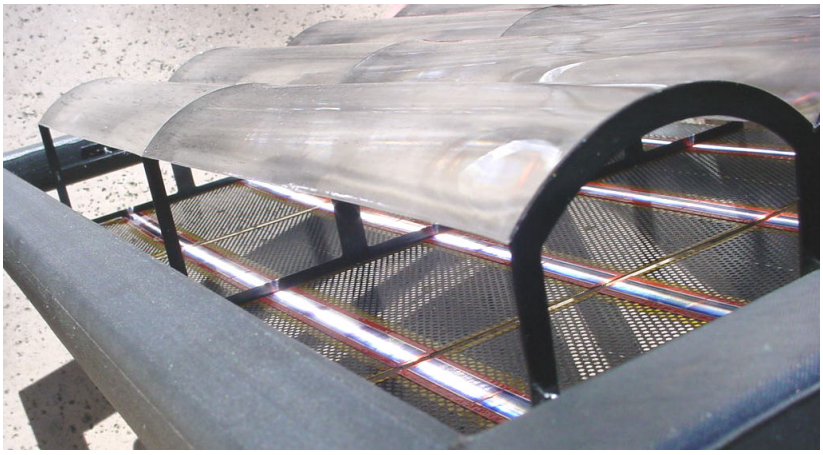

Figure 36. Optical Verification of Phase 1 SLASR Demonstration Blanket

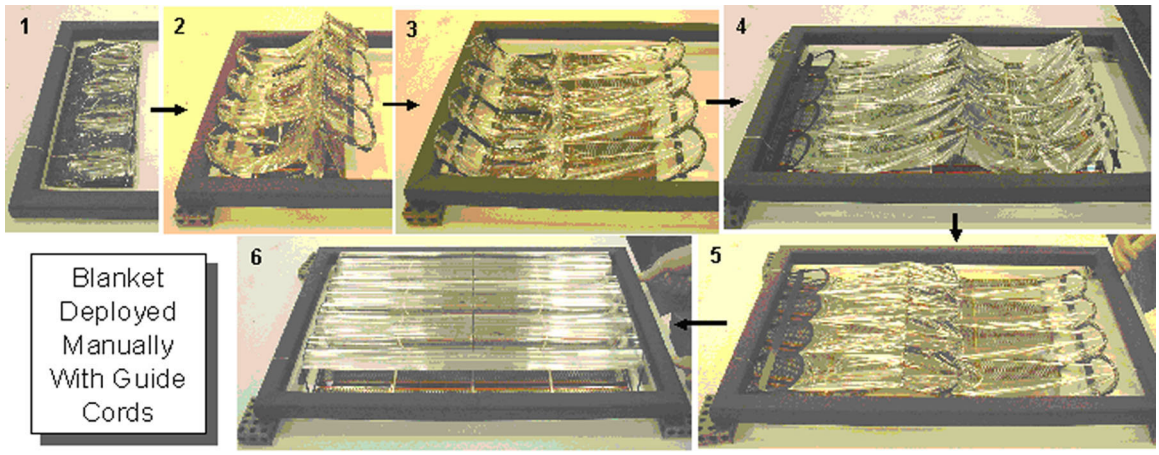

Figure 37. Phase 1 SLASR Demonstration Blanket Deployment

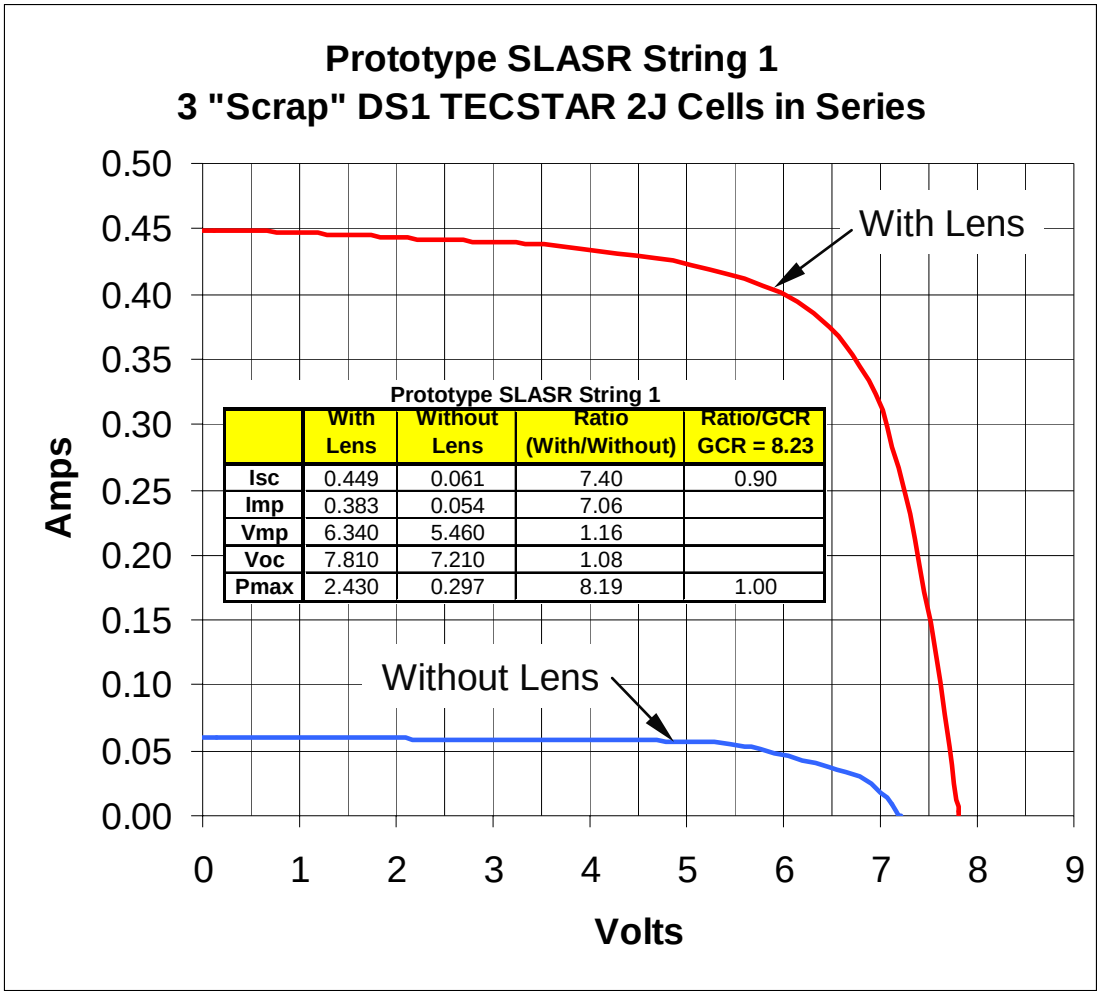

Prototype SLASR String 1

	With Lens	Without Lens	Ratio (With/Without)	Ratio/GCR GCR = 8.23
Isc	0.449	0.061	7.40	0.90
Imp	0.383	0.054	7.06	
Vmp	6.340	5.460	1.16	
Voc	7.810	7.210	1.08	
Pmax	2.430	0.297	8.19	1.00

Figure 38. Phase I SLASR Demonstration Blanket LAPSS Data

3.8 ACKNOWLEDGMENT

This work was administered though the NASA Glenn Research Center and funded by the NASA SBIR Phase 1 program under contract #NAS3-03017.

3.9 SLASR SUMMARY

Excellent progress has been made in integrating a Stretched Lens Array photovoltaic blanket into the SquareRigger solar array structure. The result is an extremely lightweight, high efficiency, high power, high voltage, and low stowed volume solar array that may enable numerous future NASA missions such as Space Solar Power (SSP), high-power deep space SEP probes, Solar Electric Propulsion (SEP) tugs and large earth-orbiting science satellites.

REFERENCES:

1) S. White, M. Douglas, B. Spence, P. Jones and M. Piszczor, “Development of an UltraFlex-Based Thin Film Solar Array for Space Applications”, 3rd WCPEC, May 2003 with, and of GRC.

2) D. Murphy, M. Eskenazi, B. Spence & P. Jones, “Thin Film & Crystalline Solar Cell Array Performance Comparisons, IEEE Conference, 2002.

3) P. Jones, J. Harvey, S. White & B. Smith, “A High Specific Power Solar Array for Low to Mid Power Spacecraft”, SPRAT Conference, 1994.

4) D. B. Snyder, "Dynamic Interactions Between Ionospheric Plasma and Spacecraft," 75th Anniversary U.R.S.I. Symposium, Brussels, Belgium, 26-27 April 1995.

5) M. Kruer and J. Lyons, "The FAST Solar Array: Challenging Requirements, Novel Design," 1st World Conference on Photovoltaic Energy Conversion, December 5-9, 1994.

6) S. Davis, R. Stillwell, W. Andiario, D. Snyder, and I. Katz, "EOS-AM Solar Array Arc Mitigation Design," 1999 Intersociety Energy Conversion Engineering Conference, Vancouver, BC Canada, August 2-6, 1999.

7) T.G. Stern, et. al., “Development of an Electrostatically Clean Solar Array Panel”, IEEE Conference, 2002.

8) B. Spence, D. Murphy, P. Jones, and M. Eskenazi, “The SCARLET Array for High Power GEO Satellites, 26th IEEE Photovoltaic Specialists Conference, September 1997.

9) O’Neill, M., et al, The Stretched Lens Array (SLA): A Low-Risk, Cost-Effective Concentrator Array Offering Wing-Level Performance of 180 W/kg and 300 W/m^2 at 300 VDC, Proceedings of the 37th Intersociety Energy Conversion Engineering Conference, July 29–31, 2002, Washington, DC IECEC 2002 Paper No. 20115.